Astronomy & Astrophysics manuscript no. EBOSS.R2.arXiV.140415
April 17, 2015

E-BOSS: An Extensive stellar BOw Shock Survey.

II. Catalogue second release

C. S. Peri[1,2,⋆], P. Benaglia[1,2,⋆⋆], N. L. Isequilla[2]

[1] Instituto Argentino de Radioastronomía, CCT-La Plata (CONICET), C.C.5, (1894) Villa Elisa, Argentina
e-mail: cperi@fcaglp.unlp.edu.ar
[2] Facultad de Ciencias Astronómicas y Geofísicas, UNLP, Paseo del Bosque s/n, (1900) La Plata, Argentina

Received July 25, 2014; accepted February 23, 2015

ABSTRACT

Context. Stellar bow shocks have been studied not only observationally, but also theoretically since the late 1980s. Only a few catalogues of them exist. The bow shocks show emission along all the electromagnetic spectrum, but they are detected more easily in infrared wavelengths. The release of new and high-quality infrared data eases the discovery and subsequent study of new objects.
Aims. We search stellar bow-shock candidates associated with nearby runaway stars, and gather them together with those found elsewhere, to enlarge the list of the E-BOSS first release. We aim to characterize the bow-shock candidates and provide a database suitable for statistical studies. We investigate the low-frequency radio emission at the position of the bow-shock features, that can contribute to further studies of high-energy emission from these objects.
Methods. We considered samples from different literature sources and searched for bow-shaped structures associated with stars in the Wide-field Infrared Survey Explorer (WISE) images. We looked for each bow-shock candidate on centimeter radio surveys.
Results. We reunited 45 bow-shock candidates and generated composed WISE images to show the emission in different infrared bands. Among them there are new sources, previously studied objects, and bow shocks found serendipitously. Five bow shocks show evidence of radio emission.
Conclusions. Stellar bow shocks constitute an active field with open questions and enormous amounts of data to be analyzed. Future research at all wavelengths databases, and use of instruments like Gaia, will provide a more complete picture of these objects. For instance, infrared spectral energy distributions can give information about physical parameters of the bow shock matter. In addition, dedicated high-sensitivity radio observations can help to understand the radio-γ connection.

Key words. Catalogs – Infrared: ISM – Stars: early-type

1. Introduction

High-mass stars interact with the interstellar medium (ISM) producing different kinds of observable structures. An important proportion of early-type (OB) stars are runaway and have high velocities with respect to the normal stars, nearby ISM, and mean Galactic rotation speed (Blaauw 1961; Gies & Bolton 1986; Gies 1987; Stone 1991; Tetzlaff et al. 2011; Fujii & Portegies Zwart 2011).

Some runaway stars generate the so-called stellar bow shocks, a comma-shaped source usually detected in front of the star trajectory. The stellar motion with respect to the ISM helps to accumulate the matter ahead of the star, and the stellar ultraviolet radiation field heats the dust that emits infrared (IR) photons (e.g., van Buren & McCray 1988; Noriega-Crespo et al. 1997; Kobulnicky et al. 2010; Gvaramadze et al. 2014). Additionally, the supersonic motion of a star produces shock waves, and through mechanisms like Fermi of first order, the charged particles can be accelerated up to relativistic velocities. These particles can interact with different fields –matter, magnetic, or photon fields– and produce high energy and radio emission (Benaglia et al. 2010; del Valle & Romero 2012; del Valle et al. 2013; del Valle & Romero 2014; López-Santiago et al. 2012). The stellar UV field also ionizes the gas, which recombines and emits photons in the optical range (Brown & Bomans 2005; Gull & Sofia 1979).

The infrared luminosity of stellar bow shocks is high compared to those in other spectral bands (e.g., Benaglia et al. 2010, Fig. 5; del Valle & Romero 2012, Fig. 11; Benaglia 2012, Table 1). Stellar bow shocks are in principle not difficult to discover at IR frequencies if they are close to us –no farther than a few kpc– and not very dim.

Among the first results of the InfraRed Astronomical Satellite (IRAS, Neugebauer et al. 1984), the first list of stellar bow shocks was published in the late 1980s. Noriega-Crespo et al. (1997) found 19 bow-shock candidates (BSCs, hereafter) and 2 doubtful objects among 58 high-mass runaway stars. The Wide-field Infrared Survey Explorer (WISE, Wright et al. 2010) satellite data release offered a sensitive arcsec resolution mid-infrared all-sky survey. In 2012, Peri et al. (2012) published the first release of the catalogue called E-BOSS: an Extensive stellar BOw Shock Survey (hereafter E-BOSS r1), done by searching these sources mainly in the then available WISE images (57% of the sky). The final product was made up of a list of 28 BSCs, and minor studies of them in radio and optical wavelengths.

In this paper, we present the E-BOSS second release (hereafter E-BOSS r2), where we extended the search to more samples. The sources taken into account are described in Section 2; the different databases used to perform the search in Section 3; and the results, including the final BSCs release 2 list, in Section

⋆ Fellow of CONICET
⋆⋆ Member of CONICET

4. Section 5 presents a discussion and Section 6 closes with a summary and conclusions.

2. Data samples: organization of the groups

E-BOSS first release (r1, Peri et al. 2012) was based on two samples. Group 1 consisted of a set of sources taken from Noriega-Crespo et al. (1997) and Group 2 was a list extracted from Tetzlaff et al. (2011). To build the present and second E-BOSS release (r2) we used samples extended to other spectral types, sources with no public WISE data at the moment of making E-BOSS r1, bow shocks from the literature, and bow shocks found serendipitously. In order to avoid confusion about the group numbers of r1 and r2, we begin here with Group 3. We give a first approximation for each group origin in this section; then we give a detailed analysis in the Results section.

2.1. Group 3

Tetzlaff et al. (2011) generated a catalogue of runaway stars using as the main source the *Hipparcos* stellar catalogue (van Leeuwen 2007). The authors selected 7663 young stars up to 3 kpc from the Sun; completed the radial velocities from literature; studied peculiar spatial, radial, and tangential velocities; and estimated the runaway probability for each star of the sample. In addition, they investigated some stars that showed high velocities with respect to their environment. Previous works analyzed the runaway origin of the high-velocity stars taking into account only peculiar spatial velocities (Blaauw 1961; Gies & Bolton 1986), radial velocities (Cruz-González et al. 1974), or tangential velocities (Moffat et al. 1998). Instead, Tetzlaff et al. (2011) combined all the available criteria and give a list of 2547 runaway stars, increasing the amount of sources in two orders of magnitude.

Originally, E-BOSS r1 Group 2 included 244 candidates for runaway stars from Tetzlaff et al. (2011). The stellar spectral types range from O to B2, and 80 of them had no public WISE data at the moment of the first release. These 80 stars form Group 3 in this paper. We named the group Tetzlaff WISE 2, because the public IR data corresponds to the second WISE release. The list of Group 3 stars is shown in Table 1.

2.2. Group 4

Group 4 collects stars from Tetzlaff et al. (2011), but with later spectral types with respect to Groups 2 and 3. We selected stars with spectral types from B3 to B5, and called this group Tetzlaff B3-B5. The list is in Table 2 and has a total of 234 stars.

2.3. Group 5

Maíz-Apellániz et al. (2004) produced an O galactic star catalogue, and classified 42 of them as runaways. We created Group 5, GOSC, with these 42 objects, and show the list in Table 3. There are two subgroups in Group 5; the first corresponds to stars already analyzed in E-BOSS r1, and the second to stars studied in this paper.

2.4. Group 6

Hoogerwerf et al. (2001) have studied the dynamic origin of 56 runaway stars and 9 pulsars. Of the 56 stars, we eliminated those coincident with the rest of the groups (from 1 to 5), and find 10 new objects to analyze. The list is presented in Table 4, labeled as Group 6, and named Hoogerwerf et al. (2001).

2.5. Group 7

We built Group 7 with BSCs already analyzed by colleagues (38 objects) and BSCs that appeared serendipitously in the IR images during our searches (7 objects). This group is called 'Serendipity and literature'. In Table 5, we enumerate the objects, list the identification in the original work (whenever possible), and characterize the WISE emission. The first column shows the name we gave to the sources in this group. We used the prefix G7 for each object and added a number that goes from 01 to 45. The last column has a comment about the region, or important information from the cited papers or added by us.

For Groups from 2 to 6 we selected runaway stars and searched for BSCs around them. In Group 7 (and Group 1, from r1) this criterion was not valid; the BSCs structures were discovered directly by us or by other authors.

2.6. Wolf-Rayet stars

The Tetzlaff et al. (2011) catalogue includes a group of Wolf-Rayet stars in the analysis of possible runaway stars. The authors list as runaways the 18 stars WR 2, 11, 15, 24, 31, 46, 47, 52, 66, 79, 110, 111, 121, 136, 138, 139, 153, and 156 (see van der Hucht 2001 for coordinates). We looked for IR bow-shaped emission at the WISE image cutouts and found no BSC related to the mentioned stars. The findings can be summarized as emission from discrete sources (WR 24, WR 153), high noise level (WR 111), wind bubble (WR 136 related to NGC 6888), and no emission above the noise for the rest of the runaway WR stars.

3. Searches

Previous evidence showed that stellar bow shocks have high infrared luminosity (e.g., Benaglia et al. 2010, Fig. 5; del Valle & Romero 2012, Fig. 11; Benaglia 2012, Table 1) compared to those in other wavelengths, which is why we aimed the search at infrared frequencies. The WISE second release (Wright et al. 2010) was published after E-BOSS r1 and completed the all-sky survey, allowing us to continue with BSCs studies.

We made use of the InfraRed Science Archive service[1] (IRSA/IPAC NASA), and performed the search seeking a bow-shock shape in front of each selected runaway star or BSC already observed, for all the r2 Groups (3 to 7). We looked for the BS structure for each source in WISE four bands, and used the FITS images already processed. The extent of the fields was one square degree. At least two authors inspected the results.

We show a RGB (red-green-blue) composed image of the resulting BSCs, except those cases where the sources had an associated WISE image already published. The RGB image shows the emission of the WISE bands 1, 3, and 4 (3.4 μm, 12.1 μm, and 22 μm, respectively). In particular, WISE band 4 is useful for detecting warm dust (Wright et al. 2010).

We investigated the final list of BSCs in radio wavelengths. The case of BD +43° 3654 (Benaglia et al. 2010) is the first BSC with synchrotron emission; we checked whether any of the new BSCs constituted a similar case. We looked for BSCs in the NRAO/VLA Sky Survey[2] (NVSS, Condon et al. 1998), which

[1] http://irsa.ipac.caltech.edu/

[2] http://www.cv.nrao.edu/nvss/postage.shtml

Table 1. Group 3: Tetzlaff WISE 2.

HIP	Sp.t.	HIP	Sp.t.	HIP	Sp.t.	HIP	Sp.t.	HIP	Sp.t.	HIP	Sp.t.
3013	B2	38518	B0.5Ib	39429	O8Iaf	39776	B2.5III	40341	B2V	41168	B2IV
41463	B2V	41878	B1.5Ib	42316	B1Ib	42354	B2III	43158	B0II/III	43868	B1Ib
44251	B2.5V	44368	B0.5Ib	46950	B1.5IV	47868	B0IV	48469**	B1V	48527	B2V
48730	B2IV-V	48745	B2III	49608	B1III	49934	B2IV	50899	B0Iab/Ib	51624	B1Ib
52526	B0Ib	52849	O9V	52898	B2III	54179	B1Iab	54475	O9II	58587	B2IV
61958	Op	65388	B2	74368	B0	89902	B2V	94716	B1II-III	97045	B0V
97845	B0.5III	98418	O7	98661	B1Iab	99283	B0.5IV	99303	B2.5V	99435	B0.5V
99580	O5e	99953	B1V	100088	B1.5V	100142	B2V	100314	B1.5Ia	100409	B1Ib
101186*	O9.5Ia	101350	B0V	102999	B0IV	103763	B2V	104316	O9	104548	B1V
104579	B1V	104814	B0.5V	105186	O8	105912	B2II	106620	B2V	106716	B2V
107864	Op	108911	B2Iab	109051	B2.5III	109082	B2V	109311	B1V	109332	B2III
109556	B1II	109562	O9Ib	109996	B1II	110025	B2III	110287	B1V	110362	B0.5IV
110386	B2IV-V	110662	B1.5IV-V	110817	B0.5Ib	111071**	B0IV	112482	B1II	112698	B1V
114482	O9.5Iab	114685	O7								

Notes. Stars from E-BOSS r1 Group 2 without WISE observations: 80 sources (identified by *Hipparcos* number). Spectral types (Sp. t.) range from O to B2, and were taken from Tetzlaff et al. (2011). Shaded in gray: 6 bow-shock candidates. (*): analyzed on E-BOSS r1 using MSX data, (**): special cases, see Section 4.5.

returns images of the 1.4 GHz frequency emission in several formats.

4. Results

4.1. Bow-shock candidates: Groups 3 to 6

Group 3, Tetzlaff WISE 2 (Table 1), has 80 objects. We found six BSC and two doubtful cases. Since the group consists of runaway stars, we associated each BSC with a star name. The six cases are: HIP 44368, HIP 47868, HIP 98418, HIP 101186, HIP 104579, and HIP 105186, and are shaded in gray in Table 1. The HIP 101186 region was already studied in E-BOSS r1, but with Midcourse Space Experiment (MSX, Egan et al. 2003) cutouts; no WISE data was available in the zone at that moment. For the six BSC we built RGB images from WISE bands cutouts (Figs. 5 and 6). Cases like HIP 48469 and HIP 111071 have no clear bow-shock shapes in their surroundings; they are separated as special cases (Section 4.5) and marked with ** in Table 1.

Group 4 is also made up of runaway stars; hence, we use the star names to identify the BSCs. We found 3 BSCs and 13 special cases; they are shaded in gray and marked with **, respectively, in Table 2. The BSCs are related to HIP 17358, HIP 46928, and HIP 107789. HIP 17358 was already analyzed in E-BOSS r1. Figure 6 shows HIP 46928 and 107789. Additionally, we encountered two bow-shock features not associated with the stars in Group 4, but in the stellar fields of HIP 5569 and HIP 33987. They will be presented in next section (Figs. 10 and 11).

In Group 5 we found evidence of one BSC, identified around HD 57682. The source is shaded in gray in Table 3 and presented in Figure 6. We found one BSC in Group 6 associated with HIP 86768 (Fig. 6) and one special case around HIP 102274. Both cases are marked in Table 4, in gray and with ** respectively.

4.2. Bow-shock candidates: Group 7

Group 7 BSCs are shown in Table 5. Povich et al. (2008) reported the discovery of six infrared stellar wind bow shocks in the galactic massive star-forming regions M17 and RCW 49 from *Spitzer* GLIMPSE (Galactic Legacy Infrared Mid-Plane Survey Extraordinaire, Benjamin et al. 2003) images. We searched for them in the WISE image database. The images looked saturated, except for the BSC RCW 49 S1 (Fig. 7).

Kobulnicky et al. (2010) found ten stellar bow shocks among *Spitzer* images, in the Cygnus OB2 association, at the heart of the Cygnus-X region. An extra case is the star BD +43° 3654, studied by Comerón & Pasquali (2007), for which the authors confirm its runaway nature, but display no image. We found each BSC in WISE images, but BSCs numbers 8 and 9 are doubtful cases (Section 4.5). We show WISE images in Figures 7 and 8, and add the BSCs in the final E-BOSS r2 list. The WISE first release did not cover the region of BD +43° 3654, and we show the RGB WISE composite image in this work (Fig. 8).

The next eight BSCs are located near two young clusters associated with the star-forming region NGC 6357 (Gvaramadze et al. 2011a). Seven were discovered in MSX, *Spitzer*, and WISE images. The authors presented one BSC with WISE images; hence, we constructed images for the other seven (Figs. 8 and 9) and included all eight in the E-BOSS r2 final list.

The structure and kinematics of the ISM around the runaway star HD 192281 was studied by Arnal et al. (2011). The authors found signs of the star trajectory using Canadian Galactic Plane Survey (CGPS, Taylor et al. 2003) and MSX images. We looked for similar structures in WISE images but no clear feature was found. In addition, we looked for a comma-shaped or similar emission, but with no success.

Vela X-1 (HIP 44368, Group 3) is the first case of a runaway HMXB (high-mass X-ray binary) showing a bow-shock structure ahead of its motion direction (Kaper et al. 1997). We include this source on E-BOSS r2. The star 4U 1907+09 is also a runaway object (Gvaramadze et al. 2011c) and presents a bow-shock feature (Fig. 10). This is the second BSC associated with a high-mass X-ray binary. 4U 1700-37 is a runaway high-mass X-ray binary too (Ankay et al. 2001). We did not find a clear comma-shaped structure ahead of the star in any of the WISE bands.

Gvaramadze et al. (2013) studied two massive stars possibly ejected from the NGC 3603 cluster through dynamical few-body encounters. The authors showed *Spitzer* images of the surroundings of the star J1117-6120 and its suspected original companion (a O2 If*/WN6 star, WR42e). We constructed a RGB WISE image for J1117-6120 (Figure 10); for WR42e, the field is saturated.

Table 2. Group 4: Tetzlaff B3-B5.

HIP	Sp.t.	HIP	Sp.t.	HIP	Sp.t.	HIP	Sp.t.	HIP	Sp.t.	HIP	Sp.t.
398	B3V	744	B5V	1115	B4V	1621	B3	3478**	B5V...	3887	B3Ia
4281	B5	4769	B	4902	B5	5023	B	5062	B3V	5569	B5
6775	B3	7873	B3V	9026	B5	9549	B5V	11487	B5III	11607	B5V
11894**	B3	12724	B5	13187	B3	14898	B3V	15114**	B5Ve	15180	B5III
15188	B3V	15424	B5III	15535	B3IV/V	15981	B3III	16203	B3III	16466	B4V
17358	B5III	17686	B5	18871	B3V	20860	B5V	22075	B5	24667	B3
24674	B5III	24795	B5	25066	B3V	25235	B3vw	25288	B4IVn	25777	B5
25906	B3II	25969	B5	26602	B4	26821	B4/B5III	27447	B3II	27548	B5
27683	B...	28949	B5IV	28981	B5	29213	B4V	29681	B5	29900	B5IV/V
30143	B3V	30169**	B5III	30943	B5V	31068	B3V	31642	B5III	31875	B3V
32220	B5	32269	B5/B6V	32786**	B5Iab/b	32864	B4IV	33490	B3V	33509	B5
33987	B5III	34485**	B5III	34611	B5	35013	B5V	35051	B3Vn	35217	B5III
35767	B4III	36024	B5III	36040	B5	36235	B5	36246	B5V	36323	B5V
36682	B4/B5V	37245	B3V	37345	B4III	37444	B4Iab	37524	B4V	39184	B5Vn
39776	B2/B3III	39866	B3V	39943	B4V	40430	B+...	41599	B3Vnne	41823	B3V
42038	B3V	42041	B5V	42251	B3ne	42605	B3IV/V	43057	B5Ib	43114	B3V
43589	B3Vn	43878	B5V	43955**	B3V	44105	B5	44879	B3IV/V	45014	B3III
45119	B4III	45145	B5V	45372	B5V	45563	B3	45742	B5V	45776	B5III
45817	B5Vn	46224	B4V	46296	B3V	46329	B5V	46470	B5IV/V	46928	B5
47005	B3/B4III	48440	B3IV	48547	B3/5V	48589**	B3V	48835	B3V	49281	B4:Vne
50044	B4Ve	50519	B5III	50764	B5III	51940	B5V:	52161	B5Vn	53294	B5III
53880	B5III	54082	B3III	54226	B+...	56709	B5	57669	B3V	57870	B4III
59232	B3IV	59607	B4III	60823	B3V	61602	Bp	62913**	B3Ib:	64622	B4V:ne
65020	B5III	66220	B	66291	B3p	66339	B5e	66524	B5II	67042	B4V
68247	B4III	69122	B5IV	69491	B5V	69591	B5V	69619	B3p	69978	B4IV/V
70042	B3III/IV	73020	B5V	74117	B3V	74680	B3V	74716	B3IV	75959	B3V
76416**	B5IV	78355	B5IV	80405	B4V	82596	B4III	82617	B3III	82658	B5V
82868	B3Vnpe	83629	B5III	84260	B3Vn	84282	B4IV	85159	B4IV	85357	B3III
85398	B5IV:	85919	B5IV:	87280	Bpsh	87886	B5Vn	87928	B4III	88156	B
88201	B3V	89061	B3II	89956	B4:Iae	89975	B3V	90761	B5	90992	B5III
91713	B3IV/V	92038	B5III	93396	B5	93463	B5/B6IV	93581	B4Vn	93974	B5
94157	B5V	94385**	B3V	94391	B4	94740	B5	94859	B5V	94899	B3Vn
95372	B3IV	95624	B5	95818	B5Vn	95856	B	95952	B5III	96115	B5
96254	B3III	97201	B5	97611	B5V	97680	B3V	99349	B3/B4IV	99527†	B4Ieq
99618**	B5	100296	B5	100308	B	100392	B5	100556	B3II/III	101112	B5
101634	B3	101909	B3V	102943	B5	104320	B3V	104609	B3	105164	B5V
105268**	B3IVe	105690	B5	107789	B5	108215	B3IV	108597	B5III	108975	B3V
110298	B5IV	110603	B5Iab	112790	B5V	113577	B5	114998	B5II/III	115186	B3V
115729	B3III	117100	B	117290	B5	117315	B3V	117700	B5	118214	B4Vne

Notes. Stars with spectral types from B3 to B5: 234 sources. The sources and spectral types were taken from Tetzlaff et al. (2011). (†): the star HIP 99527 has two possible spectral types, B4Ieq and K2Ib; we decided to select the first one. Many selected stars have spectral type B, and are included here. Shaded in gray there are the 3 bow-shock candidates. HIP 17358 was already studied on E-BOSS r1. The sources marked with ** show no clear bow-shock structures, and we give more details in Section 4.5.

Optical spectroscopy for the runaway blue supergiant TYC 3159-6-1 star was presented by Gvaramadze et al. (2014), together with a discussion that assumes Dolidze 7 to be its parent cluster (Cygnus-X region). The authors show a band 3 (12 μm) WISE image. We include the TYC 3159-6-1 nebulae as a BSC (Table 5).

Three BSCs were analyzed by Gvaramadze & Bomans (2008) near the NGC 6611 cluster, located in the Ser OB 1 association. NGC 6611 has possibly ejected three of its O massive stars: BD -14° 5040, HD 165319, and 'star 1'. HD 165319 (HIP 88652) was part of E-BOSS r1. For BD -14° 5040 and 'star 1', we generated RGB WISE images (Fig. 10) and included them in the E-BOSS r2 list (Table 6).

Sources G7 35 to 38 (Table 5) were shown in a Hubblesite News Center release[3]. We named the objects H1, H2, H3, and H4. Observations made by R. Sahai (HST Cycle 14 proposal 10536), using the ACS SNAPshot Survey of the HST between 2005 and 2006, were dedicated to a survey of preplanetary nebulae candidates (Sahai et al. 2007). Among the observed sources, Sahai and his team found what seemed to be four BSC.

Liu et al. (2011) developed a thorough study of the young cluster associated with the Circinius molecular cloud, and uncovered a population of YSOs in the western region of the cloud. The authors found two aggregates of YSOs, and H1 is located in the middle region between both YSO groups. Several sources from different works and wavelengths are mixed inside the WISE source associated with H1, like the Herbig-Haro object 139. Although HH 139 is embedded in the WISE source, H1 is about 4 arc seconds from HH 139 at optical wavelengths. We do not have sufficient evidence yet to confirm the stellar bow-shock nature of H1.

Source H2 seems to be related to the infrared source IRAS 20193+3448, its nearest source. This source was identified as 'a likely transitional YSO' (Magnier et al. 1999). If H2 is related

[3] http://hubblesite.org/newscenter/archive/releases/star/bow-shock/2009/03/

Table 3. Group 5: GOSC.

HIP	Sp.t.	HIP	Sp.t.	HIP	Sp.t.	HIP	Sp.t.	HIP	Sp.t.	HIP	Sp.t.
1415	O9III	11099	ON8V	11473	O9.5II-III	18350	O9.5	18614	O7.5III	22783	O9.5Ia
24575	O9.5V	27204	O9.5V	28881	O8 V	29147	O7.5V	39429	O4I	43158	O9.7Iab
50253	O9.5III	52849	O9V	69892	O8	81377	O9.5V	84588	O9.7Iab	85331	O6.5II
88469	O7.5Iab	93118	O6.5III	98530	O9.5III	99580	O5V	102999	O9V	104316	ON9V
105186	O7.5III	109556	O6I	114482	O9.5Iab						
HD	Sp.t.	HD	Sp.t.	HD	Sp.t.	HD	Sp.t.	HD	Sp.t.	HD	Sp.t.
12993	O6.5V	37043	O9III	36879	O7V	57682	O9I	60858	O8V	105056	ON9.7Ia
105627	O9II-III	116852	O9III	148546	O9Ia	153919	O6.5Ia	163758	O6.5Ia	168941	O9.5II-III
175754	O8 II	188209	O9.5Iab	191423	O9III						

Notes. Stars tagged as runaway in Maíz-Apellániz et al. (2004): 42 stars. Top: sources already analyzed on previous groups (1, 2, and 3). Bottom: sources not analyzed on any other group. Shaded in gray: bow-shock candidate.

Table 4. Group 6: Hoogerwerf et al. (2001).

HIP	Sp.t.	HIP	Sp.t.	HIP	Sp.t.	HIP	Sp.t.	HIP	Sp.t.
3881	B5V+...	20330	B5	38455	B2.5V	48943	B5V	86768	B1.5V
92609	B2II-IIIe	97774	B2III	102274**	B5	103206	B5IV	105811	B0Ib

Notes. Stars extracted from Hoogerwerf et al. (2001). We removed sources contained in groups 1 to 5, and 10 objects remained. Spectral types from Simbad. Shaded in gray: bow-shock candidate. Marked with **: special case.

to IRAS 20193+3448 and its surroundings, we rule out that it is a BSC, because the whole region is related to a star-forming region.

Sahai et al. (2012) published a multi-wavelength study of the source IRAS 20324+4057 and some surrounding structures; all of them near H3. They conclude the sources were dense molecular cores originated in the Cygnus cloud. Therefore, we excluded H3 as a possible BSC like the ones we are looking for.

In Hubble images H4 has a boomerang shape, but the WISE source covers several times the optical one. There is no catalogued source around H4 on about 30 arcseconds; therefore, we cannot discard the boomerang as a BSC.

Hubble Space Telescope has an angular resolution of 0.05 arcseconds, and WISE between 6.1 and 12 arcseconds depending on the band. For all the cases (H1, H2, H3, and H4), the IR sources are unresolved. Several optical sources can contribute to the IR emission. Only H4 remains as a possible BSC.

The last seven cases in Table 5 (G7 39 to 45) are serendipity BSCs. We found them in WISE images during the searches. We called the objects SER 1 to 7. SER 1 (Fig. 10) seems to have been generated by the TYC 7688-424-1 star according to Simbad sources (spectral type B5Ve). For SER 2 (Fig. 10) we do not find any catalogued star to be considered as a bow-shock producer. SER 3 (Fig. 11) could be related to HD 303197, according to Simbad. HD 303197 (spectral type B5) is located near the NGC 3324 open cluster, although the bow-shock shape seems to indicate that the star might be coming from another direction, towards the cluster. SER 4 (Fig. 11) could be produced by HIP 117265 (spectral type B2IV). SER 5 (Fig. 11) can be generated by HIP 34301 (TYC 5389-3064-1), or BD-11 1790C (double system). For SER 6 (Fig. 11) we did not find a star that might produce the BSC. SER 7 (Fig. 11) has no clear star related to it; the nearest stars are HD 153426 (80.6”), and HD 322486 (102.2”), and they are not located where runaway stars usually lie to cause a bow-shock structure.

4.3. Bow-shock candidates list

In Table 6 we list the final set of new BSCs that we found, together with those already analyzed by other authors. In E-BOSS release 2 there are 45 new objects in addition to those of release 1. The first column of Table 6 gives the name of the star that generates the BSC whenever identification was possible, or another name when the star cannot be determined. The second column contains the Group number and the third column the galactic coordinates (of stars or stagnation point), from Simbad or reference from Table 5. The stellar spectral types were taken from Simbad (B-type), the GOS Catalog (Maíz-Apellániz et al. 2004), or the reference from Table 5. The distances were taken from Megier et al. (2009), Mason et al. (1998) or were estimated using parallaxes from *Hipparcos* (van Leeuwen 2007). The stellar wind terminal velocities were interpolated or extrapolated from Table 3, Prinja et al. (1990), or adopted as in Peri et al. (2012) for stars with the same spectral types. The mass-loss rates were interpolated or extrapolated from Vink et al. (2001). The tangential velocity of HIP 44368 was estimated through proper motion values, and for the other sources of Groups 3 and 4 the values are from Tetzlaff et al. (2011). Radial velocities for Groups 3 to 6 are from Kharchenko et al. (2007); for objects in Group 7, references are as in Table 5, and Simbad for SER 1, 3, 4, and 5. Proper motions of stars in Groups 3 to 6 and K3 (HD 195229) are from *Hipparcos* (van Leeuwen 2007), and for G1 to G8 we show two values from Gvaramadze et al. (2011a); for TYC 3159-6-1, BD -14 5040, and Star 1, references are as in Table 5 (see errors for velocities and proper motions in references); for SER 1, 3, 4, and 5, Simbad.

4.4. Bow-shock candidate features

Table 7 shows the measured sizes of the bow-shock candidates. We list the length l and width w of each bow-shock structure, and distance R from the star to what is known as stagnation point (Wilkin 1996), in angular units. The sizes were taken from WISE

band 4 or band 3 images. Whenever possible, we also estimated l, w, and R on linear units (pc) through distance measurements. No size is given for cases without WISE images.

The ISM ambient density was derived for the bow-shock candidates with adopted distances and stellar spectral types, as in Peri et al. (2012). To this aim, we used the expression that gives the stagnation radius R_0:

$$R_0 = \sqrt{\frac{\dot{M} v_\infty}{4\pi \rho_a v_*^2}},$$

where $\rho_a = \mu\, n_{ISM}$ is the ambient medium density, and v_* is the spatial stellar velocity. The volume density of the ISM is in H atoms at the bow-shock position assuming $R_0 \sim R$, a mass per H atom $\mu = 2.3\times10^{-24}$ g, and the helium fractional abundance $Y = 0.1$. For those stars with unknown spatial peculiar velocity we adopted $v_* = 25$ km s^{-1}. We show the results in Table 7. Values obtained for n_{ISM} must be taken into account with caution: errors on each parameter used in the R_0 expression can have a strong influence in calculations.

4.5. Special cases

We found several doubtful cases during the BSCs search. All the special cases are marked with ** in the Tables. The cases are: in Group 3 (Table 1), HIP 48469 and 111071; in Group 4 (Table 2), HIP 3478, 11894, 15114, 30169, 32786, 34485, 43955, 48589, 62913, 76416, 94385, 99618, and 105268; in Group 6 (Table 4), HIP 102274.

In WISE band 4 (22.2 μm) many stars show circular emission around the stellar object which is usually seen in band 1, 3.4 μm. This could indicate that the radial velocity dominates over the tangential one. Other cases show different shapes depending on the WISE band, which makes us wonder if they were BSC emission or something else. In some cases, therefore, the bow shock may still be forming and has not yet achieved the comma-shape.

Group 7 (Table 5) has nine special cases. Two sources are from Kobulnicky et al. (2010): K8 and K9. The stellar bow-shock number 8 is mixed with ISM on WISE images and we did not see a clear comma-shaped object; K9 has, as many of the special cases in this work, circular emission around the star. HD 192281 (Arnal et al. 2011) images of WISE do not show a clear bow-shape either. The last special case is H4. The WISE resolution overcomes the Hubble one, precluding a BSC identification. The BSCs related to G3, G4, G6 (Gvaramadze et al. 2011a), SER3, and SER4 are doubtful cases on the basis of morphology, but we include them on the E-BOSS r2 list because they are candidates.

We do not discard any of the special cases as a probable BSC, but for the reasons stated above, we could not identify them. Subsequent studies can reveal the sources in the future and help to decide their nature.

4.6. Statistics

We carried out statistical studies for Groups 2 to 6 (E-BOSS r1 and r2) because they share the same search criterion: we looked for BSCs around runaway stars. We studied the spatial distribution and spectral types, and displayed the corresponding plots in Figures 1 and 2. We built these plots to look for trends related to stellar spectral types or spatial distribution and the presence of BSCs in the star sample.

Figure 1 shows the spatial distribution in galactic coordinates for all the sources of Groups 2 to 6, using two different symbols for the objects with or without BSCs found by us. From this figure we found no clear spatial tendencies for the sources associated with BSCs.

Figure 2 gives the total number of stars for each subspectral type, from O2 to B5, and the proportion of sources with BSCs. We had to exclude several cases; for Group 4 (stars B3-B5) we discarded sources of B type with no subspectral type, and for Group 3 (Tetzlaff WISE 2) we excluded two stars of Op type. It can be seen from the plot that the probability of finding a BSC in the surroundings of B-type stars ($\sim$ 1.2 %) is less than that for O-type stars ($\sim$ 3.6 %). This has to be taken into account of with caution because the sample of B stars in E-BOSS r2 is much larger than in r1.

4.7. Radio and high-energy emission

The first evidence of radio synchrotron emission from a stellar bow shock was presented by Benaglia et al. (2010) and it was related to the O supergiant runaway star BD +43° 3654, apparently ejected from the Cygnus OB2 association (Comerón & Pasquali 2007). The bow shock of BD +43° 3654 is the prototypical case, with matching infrared and possibly non-thermal radio emission. Synchrotron radiation reveals the presence of accelerated electrons plus a magnetic field in the bow-shock region. The accelerated electrons give rise to the possible existence of other relativistic particles. These particles can produce different non-thermal processes and high-energy photons. Benaglia et al. (2010) built a zero-order SED that fits the radio emission and predicted the detectability at shorter wavelengths. Different observational studies and models have explored this idea on other runaway stars:, ζ Ophiuchi, AE Aurigae, and HD 195592 (Terada et al. 2012; del Valle & Romero 2012; López-Santiago et al. 2012; del Valle et al. 2013). Non-thermal radiative emission models developed for these cases indicate that high-energy photons are mainly produced by the inverse Compton process (relativistic electrons interacting with IR dust photons). Moreover, the bow shock around HD 195592, is apparently related to the *Fermi* source 2FGL J2030.7+4417 (del Valle et al. 2013). In addition, runaway stars as possible variable gamma-ray sources have been studied by del Valle & Romero (2014). They found that these stars could form a set of variable gamma-ray sources switching on and off in scales of years. We looked for the final BSCs in radio databases in order to find more examples that might contribute to a better understanding of the radio-gamma connection in this kind of sources.

The NVSS VLA postage service allowed us to search for radio emission at 1.4 GHz (Condon et al. 1998) for almost all the sources. HIP 46928, SER 1, 2, and 3, and J1117-6120 were not covered by the NVSS (declination below -40 degrees). Many cases show no radio emission in the BSC region, and many others show confusing emission sources and were discarded as candidates. A few cases display very interesting features, and are perhaps related to the stellar BSCs observed at IR wavelengths. These cases are G2, G3, and SER 5. Additionally, we built images from raw data of the Australia Telescope Online Archive[4] (ATOA, project C492, Whiteoak & Uchida 1997) to examine the RCW 49 zone. We found radio emission in the BSCs RCW 49 S1 and S3. Together with three cases from E-BOSS r1 that also show radio features (HIP 88652, HIP 38430, and HIP 11891), we reunited a total of eight cases with possible radio emission

[4] http://atoa.atnf.csiro.au/

coincident with the IR radiation. Images of radio and IR emission are shown in Figures 3 and 4. The cases of RCW-49 S1 and S3 were saturated on WISE images and are not presented here.

We estimated, using the NVSS 1.4 GHz maps, noise levels and integrated fluxes over the IR WISE 4 emission regions for G2, G3, SER5, HIP 11891, HIP 24575 (AE Aur), HIP 38430, and HIP 88652. The values of noise and integrated fluxes are (in the same order as above): 4 mJy/beam, 1 mJy; 26 mJy/beam, 2 mJy; 5.5 mJy/beam, 0.5 mJy; 300 mJy/beam, 1 mJy; 1.4 mJy/beam, 0.25 mJy; 256 mJy/beam, 0.5 mJy; 22 mJy/beam, 0.4 mJy. The areas where we integrated the fluxes for NVSS do not always fully match with the IR emission exposed by WISE bands, which does not permit us to know whether all the radio emission comes from the bow-shock region. For the rest of the regions examined the noise level is ~ 0.5 mJy, which tell us that BSCs emission is lower or not-existent.

5. Discussion

Stellar bow shocks are known to be generated by high-mass early-type runaway stars, and have been identified not only in the Milky Way (e.g., Peri et al. 2012, this work) but also in the Small Magellanic Cloud (Gvaramadze et al. 2011b). Runaway stars emerge from dense clusters and are produced by two mechanisms that seem to be functioning nowadays (e.g., Hoogerwerf et al. 2001): the binary supernova scenario (BSS, Blaauw 1961) and the dynamical ejection scenario (DES, Poveda et al. 1967). Runaway stars create the possibility of exploring the existence of neutron stars in their surroundings (e.g., Hoogerwerf et al. 2001). Cases like Vela X-1 (Kaper et al. 1997) and 4U 1907+09 (Gvaramadze & Bomans 2008 and this paper) revealed that bow shocks can help to seek high-mass X-ray binaries.

Characterization of the interstellar matter can be done by means of stellar bow-shock morphology analysis. Using the stagnation point (Wilkin 1996; Peri et al. 2012), estimated by examination of the bow-shock shape and size, the medium density $n_{\rm ISM}$ can be calculated for each region of interest. We calculated $n_{\rm ISM}$ for all the BSCs that show emission in WISE band 4 or 3 and show the values in Table 7. The values of $n_{\rm ISM}$ are mostly between 0.1 and 30 cm^{-3}, and some sources show high values as 42, 44, 85, and 380 cm^{-3}. The combination of low R_0 and high $M_\odot$ can be a determining factor.

In addition, data of each bow-shock candidate in several infrared wavelengths can help to construct spectral energy distributions and compare them with dust models to estimate matter temperatures or densities (Peri et al., in preparation).

It is of great importance to compare the density values obtained with both methods because each technique has different error sources.

Many recently discovered high-energy sources (around 30%) have no identified counterparts, or more than one in other wavelengths (see, e.g., results from *Fermi* second catalogue, Nolan et al. 2012). The stellar bow shock produced by BD +43° 3654 was the first to be proposed as a possible high-energy source (Benaglia et al. 2010). Dedicated papers following this idea have been published (Benaglia et al. 2010; Terada et al. 2012; del Valle & Romero 2012; López-Santiago et al. 2012; del Valle et al. 2013), but only the case of the BSC related to HD 195592 remains as a possible high-energy (*Fermi*) source. Recently, a thorough study of *Fermi* data has been carried out by Schulz et al. (2014) for all the BSCs of E-BOSS r1 (Peri et al. 2012). The authors found no evidence of γ-ray emission in any case, and they attribute this to the possible inefficient particle acceleration or to the fact that the photon density coming from the dust is lower than assumed. Terada et al. (2012), who have found no diffuse X-ray emission for BD +43° 3654 but only an upper limit, have pointed out that it can be consequence of the low magnetic field turbulence.

Future radio observations from instruments like the Very Large Array[5] (VLA) or Giant Metrewave Radio Telescope[6] (GMRT) of the eight BSCs where we encountered NVSS 1.4 GHz emission features can help to obtain synchrotron emission parameters such as spectral indexes, and can contribute to finding better constraints of the non-thermal radiative models. In addition, deeper observations performed with instruments like *Fermi* or future ground-based arrays like CTA can give new information about the high-energy emission of stellar bow shocks and add information in similar studies.

6. Summary and conclusions

We discovered 16 new stellar bow-shock candidates and gathered 29 additional from recent literature. The 45 objects, together with those from Peri et al. (2012), form the Extensive stellar BOw Shock Survey second release. Whenever the identification was possible we present the stellar parameters of the runaway stars that probably generated them. We list the parameters of all bow-shock candidates. The complete E-BOSS list contains 73 objects.

Most of the bow-shock search consisted of investigating the surroundings of runaway stars (Groups 2 to 6). From 503 of such objects we found 27 BSCs, which represents a 5.4% rate of success. This proportion is lower than that obtained in E-BOSS r1, in which, of a total of 164 runaway stars, we encountered 17 BSCs, a success rate of 10% (only Group 2). This difference can be explained by the higher number of B-type stars sampled in this paper (Groups 2 to 6, 84 O-stars and 486 B-stars; this is in agreement with the expected number of stars of spectral types O and B for the general case). We conclude that the proportion of BSCs among O-type stars (~ 3.6 %) is larger than for B-type stars (~ 1.2 %). This can be associated with the high values of several parameters for O-type stars, such as mass-loss rates, intense UV photon fields, temperature, and wind terminal velocity. Moreover, physical conditions of the ISM, as well as the relative velocities of the star and medium can affect the shape or even allow or preclude the formation of the bow shock.

The sizes of the BSCs are similar to those observed on E-BOSS r1. The shapes are variable: typical bow shape (e.g., K5, BD +43° 3654, or HIP 101186), layered shells (SER 1, for example), asymmetric, or cases that might be showing evidence of ISM inhomogeneities.

Further exploration of IR databases and new observations of instruments like Gaia[7] will contribute to enlarging the sample of stellar bow shock and runaway stars.

Acknowledgements. C.S. Peri and P.B. are supported by the ANPCyT PICT-2012/00878. P.B. also acknowledges support from CONICET PIP 0078 and UNLP G11/115 projects. This publication makes uses of the NASA/IPAC Infrared Science Archive, which is operated by the Jet Propulsion Laboratory, California Institute of Technology, under contract with the National Aeronautics and Space Administration. We thank the SIMBAD database, operated at CDS, Strasbourg, France, and data products from the Wide-field Infrared Survey Explorer, which is a joint project of the University of California, Los Angeles, and the Jet Propulsion Laboratory/California Institute of Technology, funded by the National Aeronautics and Space Administration. We also thank the HubbleSite, which is produced by the Space Telescope Science Institute (STScI).

[5] https://science.nrao.edu/facilities/vla

[6] http://gmrt.ncra.tifr.res.in/

[7] http://sci.esa.int/gaia

STScI is operated by the Association of Universities for Research in Astronomy, Inc. (AURA) for NASA, under contract with the Goddard Space Flight Center, Greenbelt, MD. The Hubble Space Telescope is a project of international cooperation between NASA and the European Space Agency (ESA). We thank the Hubble Legacy Archive, which is a collaboration between the Space Telescope Science Institute (STScI/NASA), the Space Telescope European Coordinating Facility (ST-ECF/ESA) and the Canadian Astronomy Data Centre (CADC/NRC/CSA). Finally, we appreciate the suggestions of A. Noriega-Crespo, and insightful discussions with M. V. del Valle and L. J. Pellizza. We thank the anonymous A&A referee for comments and suggestions that improved the article.

References

Ankay, A., Kaper, L., de Bruijne, J. H. J., et al. 2001, A&A, 370, 170
Arnal, E. M., Cichowolski, S., Pineault, S., Testori, J. C., & Cappa, C. E. 2011, A&A, 532, A9
Benaglia, P. 2012, Boletin de la Asociacion Argentina de Astronomia La Plata Argentina, 55, 43
Benaglia, P., Romero, G. E., Martí, J., Peri, C. S., & Araudo, A. T. 2010, A&A, 517, L10
Benjamin, R. A., Churchwell, E., Babler, B. L., et al. 2003, PASP, 115, 953
Blaauw, A. 1961, Bull. Astron. Inst. Netherlands, 15, 265
Brown, D. & Bomans, D. J. 2005, A&A, 439, 183
Comerón, F. & Pasquali, A. 2007, A&A, 467, L23
Condon, J. J., Cotton, W. D., Greisen, E. W., et al. 1998, AJ, 115, 1693
Cruz-González, C., Recillas-Cruz, E., Costero, R., Peimbert, M., & Torres-Peimbert, S. 1974, Rev. Mexicana Astron. Astrofis., 1, 211
del Valle, M. V. & Romero, G. E. 2012, A&A, 543, A56
del Valle, M. V. & Romero, G. E. 2014, A&A, 563, A96
del Valle, M. V., Romero, G. E., & De Becker, M. 2013, A&A, 550, A112
Egan, M. P., Price, S. D., & Kraemer, K. E. 2003, in Bulletin of the American Astronomical Society, Vol. 35, American Astronomical Society Meeting Abstracts, 1301
Fujii, M. S. & Portegies Zwart, S. 2011, Science, 334, 1380
Gies, D. R. 1987, ApJS, 64, 545
Gies, D. R. & Bolton, C. T. 1986, ApJS, 61, 419
Gull, T. R. & Sofia, S. 1979, ApJ, 230, 782
Gvaramadze, V. V. & Bomans, D. J. 2008, A&A, 490, 1071
Gvaramadze, V. V., Kniazev, A. Y., Chené, A.-N., & Schnurr, O. 2013, MNRAS, 430, L20
Gvaramadze, V. V., Kniazev, A. Y., Kroupa, P., & Oh, S. 2011a, A&A, 535, A29
Gvaramadze, V. V., Miroshnichenko, A. S., Castro, N., Langer, N., & Zharikov, S. V. 2014, MNRAS, 437, 2761
Gvaramadze, V. V., Pflamm-Altenburg, J., & Kroupa, P. 2011b, A&A, 525, A17
Gvaramadze, V. V., Röser, S., Scholz, R.-D., & Schilbach, E. 2011c, A&A, 529, A14
Hoogerwerf, R., de Bruijne, J. H. J., & de Zeeuw, P. T. 2001, A&A, 365, 49
Kaper, L., van Loon, J. T., Augusteijn, T., et al. 1997, ApJ, 475, L37
Kharchenko, N. V., Scholz, R.-D., Piskunov, A. E., Röser, S., & Schilbach, E. 2007, Astronomische Nachrichten, 328, 889
Kobulnicky, H. A., Gilbert, I. J., & Kiminki, D. C. 2010, ApJ, 710, 549
Liu, W. M., Padgett, D. L., Leisawitz, D., Fajardo-Acosta, S., & Koenig, X. P. 2011, ApJ, 733, L2
López-Santiago, J., Miceli, M., del Valle, M. V., et al. 2012, ApJ, 757, L6
Magnier, E. A., Volp, A. W., Laan, K., van den Ancker, M. E., & Waters, L. B. F. M. 1999, A&A, 352, 228
Maíz-Apellániz, J., Walborn, N. R., Galué, H. Á., & Wei, L. H. 2004, ApJS, 151, 103
Mason, B. D., Gies, D. R., Hartkopf, W. I., et al. 1998, AJ, 115, 821
Megier, A., Strobel, A., Galazutdinov, G. A., & Krełowski, J. 2009, A&A, 507, 833
Moffat, A. F. J., Marchenko, S. V., Seggewiss, W., et al. 1998, A&A, 331, 949
Neugebauer, G., Habing, H. J., van Duinen, R., et al. 1984, ApJ, 278, L1
Nolan, P. L., Abdo, A. A., Ackermann, M., et al. 2012, ApJS, 199, 31
Noriega-Crespo, A., van Buren, D., & Dgani, R. 1997, AJ, 113, 780
Peri, C. S., Benaglia, P., Brookes, D. P., Stevens, I. R., & Isequilla, N. L. 2012, A&A, 538, A108
Poveda, A., Ruiz, J., & Allen, C. 1967, Boletin de los Observatorios Tonantzintla y Tacubaya, 4, 86
Povich, M. S., Benjamin, R. A., Whitney, B. A., et al. 2008, ApJ, 689, 242
Prinja, R. K., Barlow, M. J., & Howarth, I. D. 1990, ApJ, 361, 607
Sahai, R., Morris, M., Sánchez Contreras, C., & Claussen, M. 2007, AJ, 134, 2200
Sahai, R., Morris, M. R., & Claussen, M. J. 2012, ApJ, 751, 69
Schulz, A., Ackermann, M., Buehler, R., Mayer, M., & Klepser, S. 2014, A&A, 565, A95
Stone, R. C. 1991, AJ, 102, 333
Taylor, A. R., Gibson, S. J., Peracaula, M., et al. 2003, AJ, 125, 3145
Terada, Y., Tashiro, M. S., Bamba, A., et al. 2012, PASJ, 64, 138
Tetzlaff, N., Neuhäuser, R., & Hohle, M. M. 2011, MNRAS, 410, 190
van Buren, D. & McCray, R. 1988, ApJ, 329, L93
van der Hucht, K. A. 2001, New A Rev., 45, 135
van Leeuwen, F. 2007, A&A, 474, 653
Vink, J. S., de Koter, A., & Lamers, H. J. G. L. M. 2001, A&A, 369, 574
Whiteoak, J. B. Z. & Uchida, K. I. 1997, A&A, 317, 563
Wilkin, F. P. 1996, ApJ, 459, L31
Wright, E. L., Eisenhardt, P. R. M., Mainzer, A. K., et al. 2010, AJ, 140, 1868

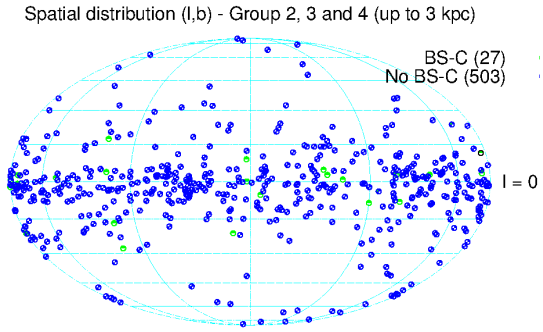

Fig. 1. Distribution on the (l,b) plane of Groups 2, 3, 4, 5 and 6. Runaway stars were taken from Tetzlaff et al. (2011) and Hoogerwerf et al. (2001).

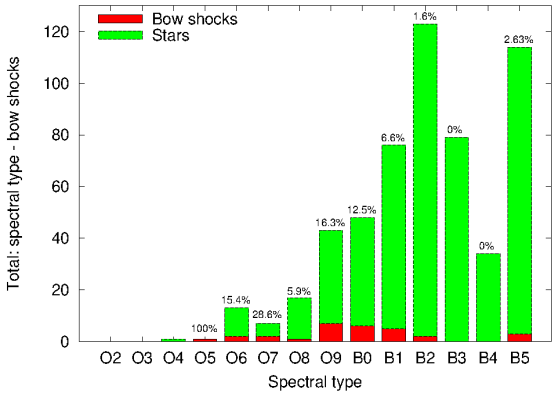

Fig. 2. Spectral type histogram for Groups 2 to 6, summarized. Each range of spectral types has the total number of stars in green, the amount of BSCs in red, and the proportion of BSCs according to the total number of sources in each range. We did not include stars of spectral types with no specific subtype (two stars of spectral type Op, and 12 stars of spectral type B).

Table 5. Group 7: Serendipity and literature.

Number	Name	RA (J2000)	DEC (J2000)	Ref.	WISE	Figure	Comments
G7-01	M17-S1	18:20:22.72	-16:08:34.27	A	•	–	M17 region
G7-02	M17-S2	18:20:25.88	-16:08:32.48	A	•	–	M17 region
G7-03	M17-S3	18:20:26.63	-16:07:08.55	A	•	–	M17 region
G7-04	RCW 49-S1	10:22:23.06	-57:44:27.92	A	⊃	Fig. 7	RCW 49 region
G7-05	RCW 49-S2	10:24:03.12	-57:48:36.00	A	•	–	RCW 49 region
G7-06	RCW 49-S3	10:24:39.18	-57:45:20.97	A	•	–	RCW 49 region
G7-07	K1	20:34:28.9	+41:56:17.0	B	⊃	Fig. 7	Cygnus-X region
G7-08	K2	20:34:34.5	+41:58:29.3	B	⊃	Fig. 7	Cygnus-X region
G7-09	K3	20:28:30.2	+42:00:35.2	B	⊃	Fig. 7	Cygnus-X region
G7-10	K4	20:28:39.4	+40:56:51.0	B	⊃	Fig. 7	Cygnus-X region
G7-11	K5	20:34:55.1	+40:34:44.0	B	⊃	Fig. 7	Cygnus-X region
G7-12	K6	20:36:13.3	+41:34:26.1	B	⊃	Fig. 8	Cygnus-X region
G7-13	K7	20:36:04.4	+40:56:13.0	B	⊃	Fig. 8	Cygnus-X region
G7-14**	K8	20:20:11.6	+39:45:30.1	B	?	–	Cygnus-X region, Special case
G7-15**	K9	20:25:43.9	+38:11:13.2	B	?	–	Cygnus-X region, Special case
G7-16	K10	20:29:22.1	+37:55:44.3	B	⊃	Fig. 8	Cygnus-X region
G7-17*	K11	20:33:36.1	+43:59:07.4	B	⊃	Fig. 8	Cygnus-X region, BD +43° 3654
G7-18	G1	17:27:11.23	-34:14:34.9	C	⊃	Fig. 8	NGC 6357 region
G7-19	G2	17:22:03.43	-34:14:24.1	C	⊃	Fig. 8	NGC 6357 region
G7-20**	G3	17:28:21.67	-34:32:30.3	C	⊃	Fig. 9	NGC 6357 region, HD 319881
G7-21**	G4	17:18:15.40	-34:00:06.1	C	⊃	Fig. 9	NGC 6357 region, New RGB figure
G7-22	G5	17:22:05.62	-35:39:55.5	C	⊃	Fig. 9	NGC 6357 region, [N78] 34
G7-23**	G6	17:22:50.02	-34:03:22.4	C	⊃	Fig. 9	NGC 6357 region
G7-24	G7	17:27:12.53	-33:30:40.0	C	⊃	Fig. 9	NGC 6357 region
G7-25	G8	17:24:05.62	-34:07:09.5	C	⊃	Fig. 9	NGC 6357 region
G7-26**	HD 192281	20:12:33.12	+40:16:05.45	D	?	–	Special case
G7-27*	Vela X-1	09:02:06.86	-40:33:16.9	E, F	⊃	Fig. 5	HIP 44368, Group 3, HMXB
G7-28	4U 1907+09	19:09:37.9	+09:49:49	F	⊃	Fig. 10	HMXB
G7-29	4U 1700-37	17:03:56.77	-37:50:38.92	G	?	–	HMXB
G7-30	J1117-6120	11:17:12.93	-61:20:08.6	H	⊃	Fig. 10	NGC 3603 region
G7-31	TYC 3159-6-1	20:18:40.37	41:32:45	I	⊃	–	Cygnus-X region
G7-32	BD -14 5040	18:25:38.9	-14:45:05.74	J	⊃	Fig. 10	NGC 6611 region
G7-33*	HD 165319	18:05:58.84	-14:11:52.9	J	⊃	–	NGC 6611 region, HIP 88652, Group 2
G7-34	Star 1	18:15:23.97	-13:19:35.8	J	⊃	Fig. 10	NGC 6611 region
G7-35	H1	15:00:58.55	-63:16:54.7	K	†	–	Near: YSO and HH 139
G7-36	H2	20:21:18.99	+34:57:50.96	L	†	–	Probable YSO
G7-37	H3	20:34:12.92	+41:08:15.94	M	†	–	EGGs (evaporating gaseous globules)
G7-38**	H4	05:46:51.51	+25:03:48.18		⊃?	–	Probable BSC?
G7-39	SER1	08:58:29.4	-43:25:09		⊃	Fig. 10	Probably produced by TYC 7688-424-1
G7-40	SER2	10:03:42	-58:30:28		⊃	Fig. 10	Not clear
G7-41**	SER3	10:38:19	-58:53:22		⊃	Fig. 11	Probably produced by HD 303197
G7-42**	SER4	23:46:37	+66:46:20		⊃	Fig. 11	Probably produced by HIP 117265
G7-43	SER5	07:06:33.6	-11:17:24.5		⊃	Fig. 11	Probably produced by HIP 34301
G7-44	SER6	01:11:24.3	+57:33:38		⊃	Fig. 11	Not clear
G7-45	SER7	17:01:20	-38:12:24.5		⊃	Fig. 11	Not clear

Notes. Number: G7 stands for 'Group 7' and the number from 01 to 45 is specific of this table. For G7 01 to 34 we looked for bow-shock candidates in WISE images using sources from other works (references in column 5). G7 39 to 45 were serendipitously discovered during the catalogue production. (*): already analyzed in other Groups (1 to 6) of E-BOSS r1 or r2. Name: extracted from the references (A to M) for G7 01 to 34. Coordinates: for stars that produce the bow shock (whenever possible), or BSC apex coordinates estimated by us (visually), where the star could not be identified. ⊃: BS shape observed in WISE images, ⊃?: BSC to be confirmed, •: emission excess in the region of BS, ?: doubtful cases, detailed in Section Special cases, †: not enough resolution to identify bow-shock shape in WISE images. Figure: reference to the Figures in the present work. Comments: a relevant comment for each case. References in column 5; A: Povich et al. (2008), B: Kobulnicky et al. (2010), C: Gvaramadze et al. (2011a), D: Arnal et al. (2011), E: Kaper et al. (1997), F: Gvaramadze et al. (2011c), G: Ankay et al. (2001), H: Gvaramadze et al. (2013), I: Gvaramadze et al. (2014), J:Gvaramadze & Bomans (2008), K: Liu et al. (2011), L: Magnier et al. (1999), M: Sahai et al. (2012).

Table 6. List of the E-BOSS release 2 bow-shock candidates and corresponding stellar parameters.

Source	Gr.	l [°]	b [°]	Spectral type	d [pc]	v_∞ [km/s]	$\dot{M} \times 10^6$ [$M_\odot$/yr]	v_{tg} [km/s]	v_r [km/s]	$\mu_\alpha \cos\delta$ [mas/yr]	μ_δ [mas/yr]
HIP 44368[1]	3,7	263.1	+3.9	B0.5 Iab	1900±0.1[z]	1100	0.8	52.2	-1.00	-5.5	8.8
HIP 46928	4	295.6	-21.04	B5V	[175.44]	100	0.03	13.6	-42.00	-34.81	14.18
HIP 47868	3	261.8	+17.4	B0.5IIIn	[1075.27]	1200	0.3	29.5	31.70	-11.44	5.92
HIP 98418	3	71.6	+2.9	O7	[529.10]	2545	0.24	21.8	20.00	-5.56	-9.59
HIP 104579	3	81.0	-8.07	B1Vp	[1149.42]	650	0.03	26.6	-6.00	0.37	0.53
HIP 105186	3	87.6	-3.8	O8e	1130±190[a]	2340	0.1	57.0	-30.00	4.85	-8.40
HIP 107789	4	102.1	+4.8	B5	[1190.47]	100	0.03	16.3	-16.00	-1.5 1	-5.07
HD 57682	5	224.4	+2.6	O9 IV	1600[b]	1900	0.16	–	24.10	10.46	13.38
HIP 86768	6	18.7	+11.6	B1.5V	737[a]	[550]	0.03	–	-26	-4.32	-10.60
M17-S1	7	15.07	0.64	O9-B2V	1600[z]	1000	0.03	–	–	–	–
M17-S2	7	15.08	0.65	O7-O8V	”	[1500]	0.16	–	–	–	–
M17-S3	7	15.10	0.64	O7V	”	2300	0.25	–	–	–	–
RCW 49-S1	7	284.08	0.43	O5III	6100[z]	2800	3.23	–	–	–	–
RCW 49-S2	7	284.30	0.3	O6 V	”	2600	0.6	–	–	–	–
RCW 49-S3	7	284.34	0.2	O3V/O6.5III	”	2800	2	–	–	–	–
K1	7	80.86	0.97	O9V	1500[z]	1500	0.05	–	-17 ± 6	–	–
K2	7	80.90	0.98	B1V-B3V	”	500	0.03	–	-12 ± 15	–	–
K3	7	80.26	1.91	B0.2III	”	[1250]	0.1		-3 ± 2	-0.22	3.84
K4	7	79.42	1.28	B2V-B3V	”	[300]	0.03	–	–	–	–
K5	7	79.82	0.09	O9V	”	1500	0.05	–	10 ± 10	–	–
K6	7	80.76	0.49	B4V-B6V	”	250	0.03	–	–	–	–
K7	7	80.24	0.14	O5V	”	2500	1.5	–	–	–	–
K8	7	77.52	1.90	B1V-B3V	”	[400]	0.03	–	2 ± 4	–	–
K9	7	76.84	0.12	B?	”	400	0.03	–	–	–	–
K10	7	77.05	-0.61	B1V-B2V	”	[550]	0.03	–	–	–	–
G1	7	353.42	0.45	O7.5-O7V	1700[z]	2100	0.2	–	–	-1.5/-3.8	-1.6/-5
G2	7	352.82	1.33	O5.5-O6.5-/V	”	2250	0.4	–	–	-8.5/-8.9	-3.2/-11.3
G3	7	353.30	0.08	O6Vn-O5V	”	2000	0.4	–	–	0/3.4	-2.8/-3.2
G4	7	352.57	2.11	O6.5-O6V	”	2550	0.5	–	–	-4.4/-9	0.9/2.3
G5	7	351.65	0.51	O8/B0III/V-O6.5V	”	2000	0.1	–	–	-4.9/-11.8	11.7/18.7
G6	7	353.06	1.29	B0V	”	[1000]	0.1	–	–	-4.6/-8.1	0.8/0.1
G7	7	354.03	0.85	B0V	”	[1000]	0.1	–	–	-3.9/-7.3	0.0/-3.2
G8	7	353.16	1.05	O9-9.5V	”	[1500]	0.04	–	–	-6.0/-9.4	1.9/-2.5
4U 1907+09	7	43.74	0.47	O9.5 Iab	4000[z]	2900	0.7	–	–	–	–
J1117-6120	7	291.88	-0.50	O6 V	7600[z]	2600	0.6	–	-21.4	–	–
TYC 3159-6-1	7	78.83	+3.15	O9.5-O9.7 Ib	1500[z]	2900	0.7	–	-35.8	-2.4	-0.1
BD -14 5040	7	16.89	-1.12	B	1800[z]	400	0.03		–	5.5/7.7	-3.0/-4.6
Star 1	7	16.98	1.75	O9.5III/O5V–O7.5III/O4V	1800[z]	2200	0.63		–	0/-4.3	12/0.9
SER1	7	264.78	1.54	B5 Ve	–	250	0.03	–	–	-9.5	8.5
SER2	7	282.48	-2.46	–	–	–	–	–	–	–	–
SER3	7	286.46	-0.34	B5 (V)	–	250	0.03	–	–	–	–
SER4	7	116.59	4.70	B2 IV	–	500	0.03	–	-9.7	8.71	-3.59
SER5	7	224.69	-1.82	B0.5IV	–	550	0.03	–	31	-3.14	3.32
SER6	7	125.62	-5.20	–	–	–	–	–	–	–	–
SER7	7	347.15	2.36	–	–	–	–	–	–	–	–

Notes. Column 1: star names for the identified cases or name given by us; (1): Vela X-1. Column 2: group number for each object. Galactic coordinates l,b: from Simbad or corresponding references for Group 7 sources (Table 5, fifth column). Spectral types: for B-type stars from Simbad; for O-type stars (whenever possible) from GOS Catalog (Maíz-Apellániz et al. 2004), otherwise from same reference as in Table 5. For SER 2, 6, and 7 we did not find stars related. Distances: (a) Megier et al. (2009), (b) Mason et al. (1998), (z) from same references of Table 5; []: derived from *Hipparcos* parallaxes (van Leeuwen 2007). Wind terminal velocities: inter or extrapolated from Table 3, Prinja et al. (1990); []: as adopted in Peri et al. (2012) for stars with same spectral types. Mass loss rates: inter or extrapolated from Vink et al. (2001). Tangential velocities: for HIP 44368 estimated through proper motion values; for the other sources of groups 3 and 4 from Tetzlaff et al. (2011). Radial velocities: for groups 3 to 6, from Kharchenko et al. (2007); for objects from Group 7, references as in Table 5, and Simbad for SER 1, 3, 4, and 5. Proper motions: for groups 3 to 6, and K3 (HD 195229), from van Leeuwen (2007); for G1 to G8 we show two values from Gvaramadze et al. (2011a); for TYC 3159-6-1, BD -14 5040, and Star 1, reference as in Table 5 (see errors for velocities and proper motions in references); for SER 1, 3, 4, and 5, Simbad.

Table 7. Parameters of the bow-shock candidates and medium density.

Source	l	w	R	l	w	R	$n_{\rm ISM}$	Source	l	w	R	l	w	R	$n_{\rm ISM}$
	[']			[pc]			[cm^{-3}]		[']			[pc]			[cm^{-3}]
HIP 44368	5	1.25	0.8	2.76	0.69	0.44	1.8	G1	4	0.8	0.8	1.98	0.4	0.4	14
HIP 46928	1.8	0.47	1	0.09	0.02	0.05	2	G2	6	1.2	1.2	2.97	0.59	0.59	14
HIP 47868	5	1.7	1.6	1.56	0.53	0.50	2.6	G3	5	1.5	1	2.47	0.74	0.49	16
HIP 98418	1.66	0.6	0.5	0.26	0.09	0.08	380	G4	3	1	0.8	1.48	0.49	0.4	42
HIP 101186*	22	4	4.5	9.50	1.73	1.94	2.63	G5	3	1	1	1.48	0.49	0.49	4
HIP 104579	3	1.3	1.1	1.00	0.43	0.37	0.7	G6	1.5	0.5	0.4	0.74	0.25	0.2	13
HIP 105186	7	2	2.5	2.30	0.66	0.82	0.3	G7	1.5	0.5	0.3	0.74	0.25	0.15	23
HIP 107789	1.2	0.4	0.3	0.42	0.14	0.10	1.8	G8	1.5	0.5	0.5	0.74	0.25	0.25	5
BD +43°3654*	19	3	4	8.01	1.26	1.69	3.5	4U 1907+09	3.5	1	1.5	4.07	1.16	1.74	0.1
HD 57682	1.6	0.4	0.3	0.74	0.19	0.14	85	J1117-6120	1.5	0.5	0.5	3.31	1.1	1.1	6.4
HIP 86768	4	2	2	0.86	0.43	0.43	0.1	BD -14 5040	4	1	1	2.09	0.52	0.52	0.1
RCW 49-S1	2.5	0.5	0.7	4.43	0.89	1.24	30	Star 1	7	1	1.5	3.66	0.52	0.78	–
K1	3	1	0.7	1.31	0.44	0.31	4	SER1	4	1.5	1	–	–	–	–
K2	4	0.3	0.5	1.74	0.13	0.22	1.7	SER2	2.5	1	1	–	–	–	–
K3	2	0.5	0.4	0.87	0.22	0.17	16.6	SER3	2.5	0.5	0.5	–	–	–	–
K4	1	0.3	0.3	0.44	0.13	0.13	2.8	SER4	2.5	1	1	–	–	–	–
K5	4	1	1	1.74	0.44	0.44	2	SER5	6	1	2	–	–	–	–
K6	2.5	0.5	0.7	1.09	0.22	0.31	0.4	SER6	2.5	0.6	0.5	–	–	–	–
K7	5	1	1.5	2.18	0.44	0.65	44	SER7	8	1.5	1.5	–	–	–	–
K10	2	0.5	0.5	0.87	0.22	0.22	1.8								

Notes. Columns 2 to 4 and 10 to 12: length l and width w of the bow-shock structure, and distance R from the star to the midpoint of the bow shock, in angular units. The sizes were estimated from WISE band 4 (22 μm) images, and with band 3 (12.1 μm) images when identification was not clear in band 4. Columns 5 to 7 and 13 to 15: same variables as before, in linear units, for those stars of known distances. Columns 8 and 16: ambient density as derived in Peri et al. (2012) (Wilkin 1996). (*): studied in E-BOSS r1 (Peri et al. 2012) only through MSX images.

Table 8. Total list of BSC of E-BOSS r1 and r2.

ID	Name	Rel.	Group	ID	Name	Rel.	Group	ID	Name	Rel.	Group
EB01	HIP 2036	r1	2	EB26	HIP 101186	r1	1	EB51	HIP 86768	r2	6
EB02	HIP 2599	r1	1,2	EB27	BD+433654	r1	1	EB52	Star 1	r2	7
EB03	HIP 11891	r1	2	EB28	HIP 114990	r1	1	EB53	M17-S1	r2	7
EB04	HIP 16518	r1	2	EB29	SER6	r2	7	EB54	M17-S2	r2	7
EB05	HIP 17358	r1	1	EB30	SER5	r2	7	EB55	M17-S3	r2	7
EB06	HIP 22783	r1	1	EB31	HIP 57862	r2	5	EB56	BD -14 5040	r2	7
EB07	HIP 24575	r1	2	EB32	SER1	r2	7	EB57	4U 1907+09	r2	7
EB08	HIP 25923	r1	2	EB33	HIP 44368	r2	3,7	EB58	HIP 98418	r2	3
EB09	HIP 26397	r1	2	EB34	HIP 46928	r2	4	EB59	TYC 3159-6-1	r2	7
EB10	HIP 28881	r1	1	EB35	HIP 47868	r2	3	EB60	K8	r2	7
EB11	HIP 29276	r1	1,2	EB36	SER2	r2	7	EB61	K9	r2	7
EB12	HIP 31766	r1	2	EB37	RCW 49-S1	r2	7	EB62	K3	r2	7
EB13	HIP 32067	r1	1,2	EB38	RCW 49-S2	r2	7	EB63	K4	r2	7
EB14	HIP 34536	r1	1,2	EB39	RCW 49-S3	r2	7	EB64	K10	r2	7
EB15	HIP 38430	r1	1	EB40	SER3	r2	7	EB65	K1	r2	7
EB16	HIP 62322	r1	2	EB41	J1117-6120	r2	7	EB66	K2	r2	7
EB17	HIP 72510	r1	1,2	EB42	SER7	r2	7	EB67	K5	r2	7
EB18	HIP 75095	r1	1,2	EB43	G4	r2	7	EB68	K7	r2	7
EB19	HIP 77391	r1	1	EB44	G2	r2	7	EB69	K6	r2	7
EB20	HIP 78401	r1	1	EB45	G5	r2	7	EB70	HIP 104579	r2	3
EB21	HIP 81377	r1	1,2	EB46	G6	r2	7	EB71	HIP 105186	r2	3
EB22	HIP 82171	r1	2	EB47	G8	r2	7	EB72	HIP 107789	r2	4
EB23	HIP 88652	r1	2	EB48	G1	r2	7	EB73	SER4	r2	7
EB24	HIP 92865	r1	1	EB49	G7	r2	7				
EB25	HIP 97796	r1	1	EB50	G3	r2	7				

Notes. Bow-shock candidates of E-BOSS release 1 and 2 reunited. We give a specific name to the catalogue that goes from 01 to 73 with EB from E-BOSS as a prefix. There are 28 objects from r1 and 45 from r2. The Group for each source is also given.

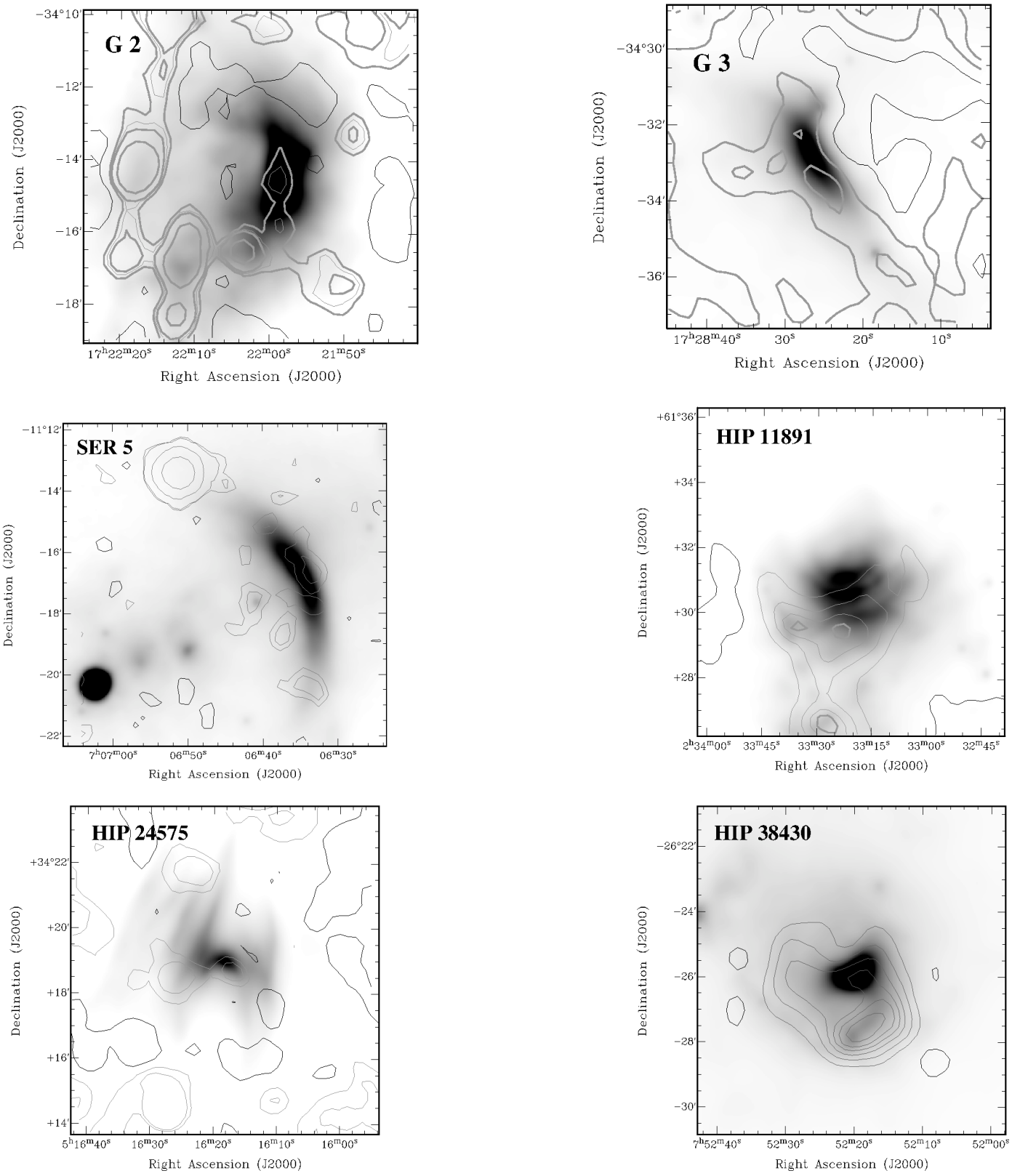

Fig. 3. BSCs that show radio emission. Gray scale colors: IR WISE emission (band 4, 22.2 μm). Contours: NVSS 1.4 GHz emission. Positive values in gray, negative in black. Contour levels on each image: *Top left*, -1, 1, 1.5, 2, 5 mJy/b. *Top right*, -5, 1, 5 mJy/b. *Middle left*, -1, 1, 1.5, 20, 150 mJy/b. *Middle right*, -4, 4, 16, 30, 40 mJy/b. *Bottom left*, -1, 1, 2, 3 mJy/b. *Bottom right*, -10, 10, 30, 60, 90, 120, 160 mJy/b.

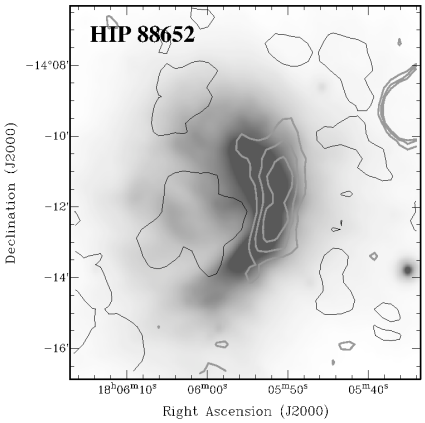

Fig. 4. Bow-shock candidate related to HIP 88652 (E-BOSS r1). Gray scale colors: IR WISE emission (band 4, 22.2 μm). Contours: NVSS 1.4 GHz emission. Contour levels: -1, 1, 2, 3 mJy/b. Positive values in gray, negative in black.

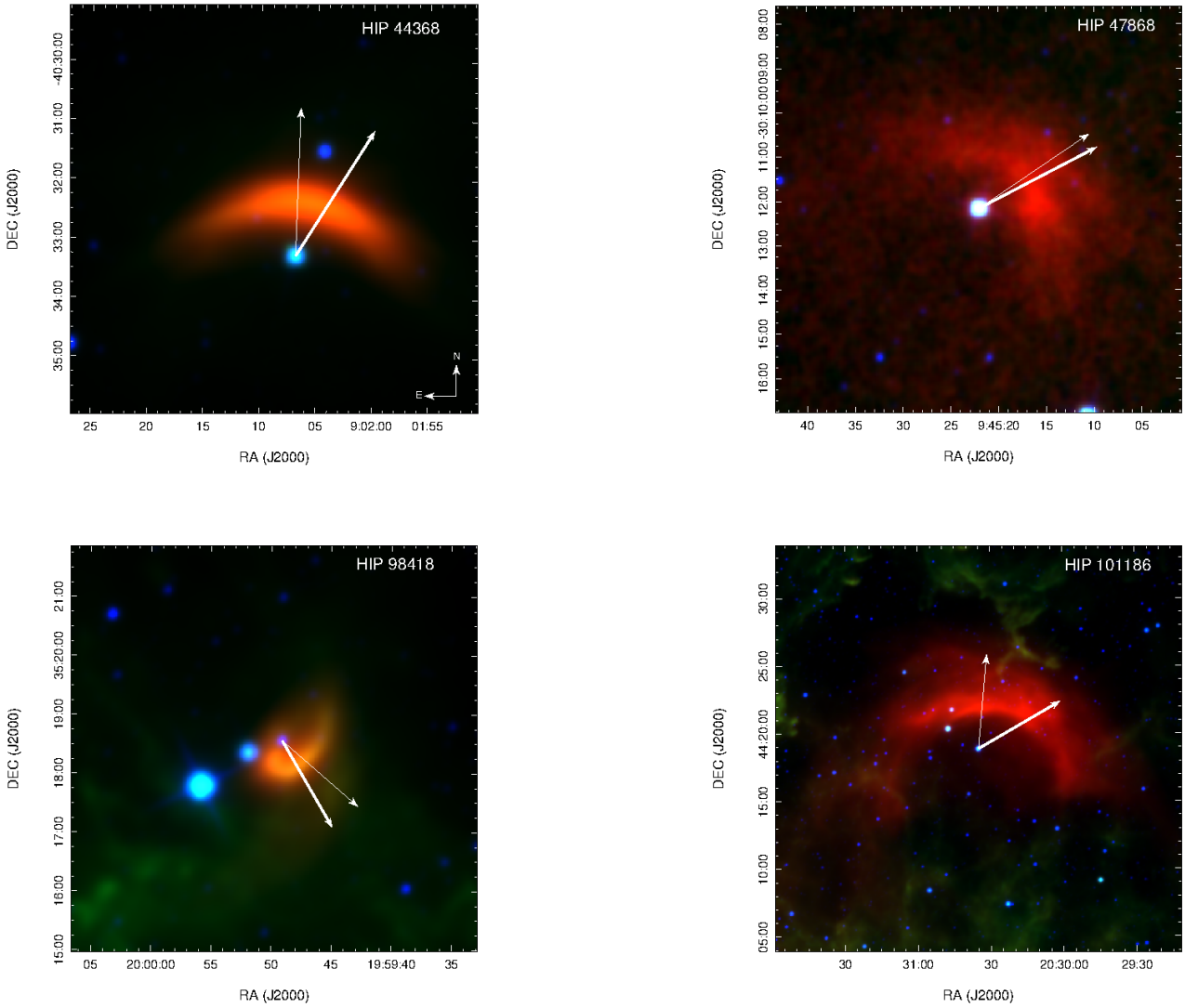

Fig. 5. Group 3 bow-shock candidates WISE images. Red: band 4, 22.2 μm. Green: band 3, 12.1 μm. Blue: band 1, 3.4 μm. The label stands for the name in the final list of E-BOSS r2 BSCs. We have drawn $\mu_\alpha \cos\delta$ and μ_δ to compose the total μ. The thick vectors represent the measured *Hipparcos* proper motions (van Leeuwen 2007), and the thinner vectors stand for the star proper motions but corrected for the ISM motion caused by Galactic rotation. The vector lengths are not scaled with the original values. Compass as in HIP 44368 is the same for all RGB images.

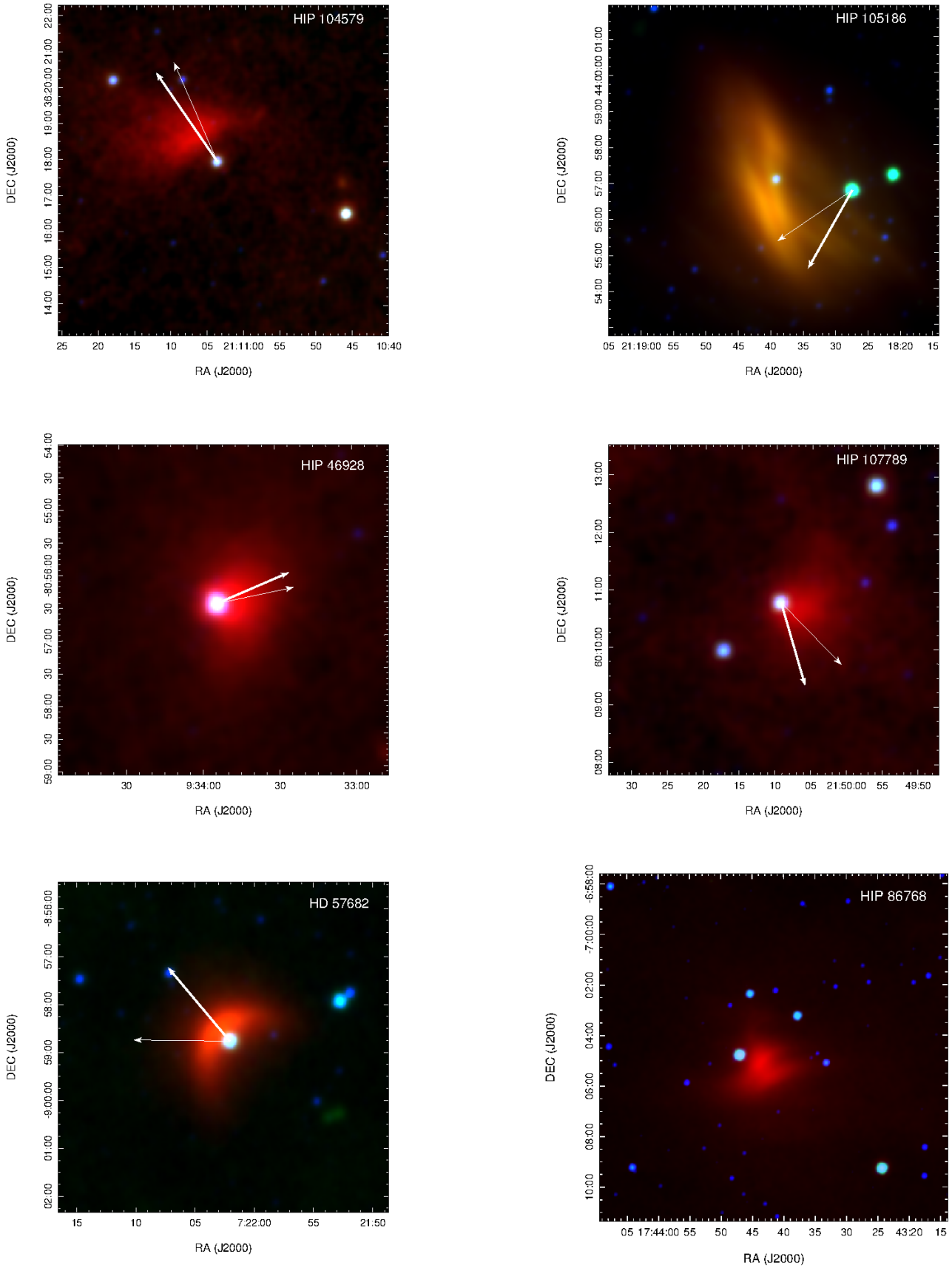

Fig. 6. Groups 3, 4, 5, and 6 bow-shock candidates WISE images. Red: band 4, 22.2 μm. Green: band 3, 12.1 μm. Blue: band 1, 3.4 μm. The label stands for the name in the final list of E-BOSS r2 BSCs. We have drawn $\mu_\alpha \cos\delta$ and μ_δ to compose the total μ. The thick vectors represent the measured *Hipparcos* proper motions (van Leeuwen 2007), and the thinner vectors stand for the star proper motions but corrected for the ISM motion caused by Galactic rotation. The vector lengths are not scaled with the original values.

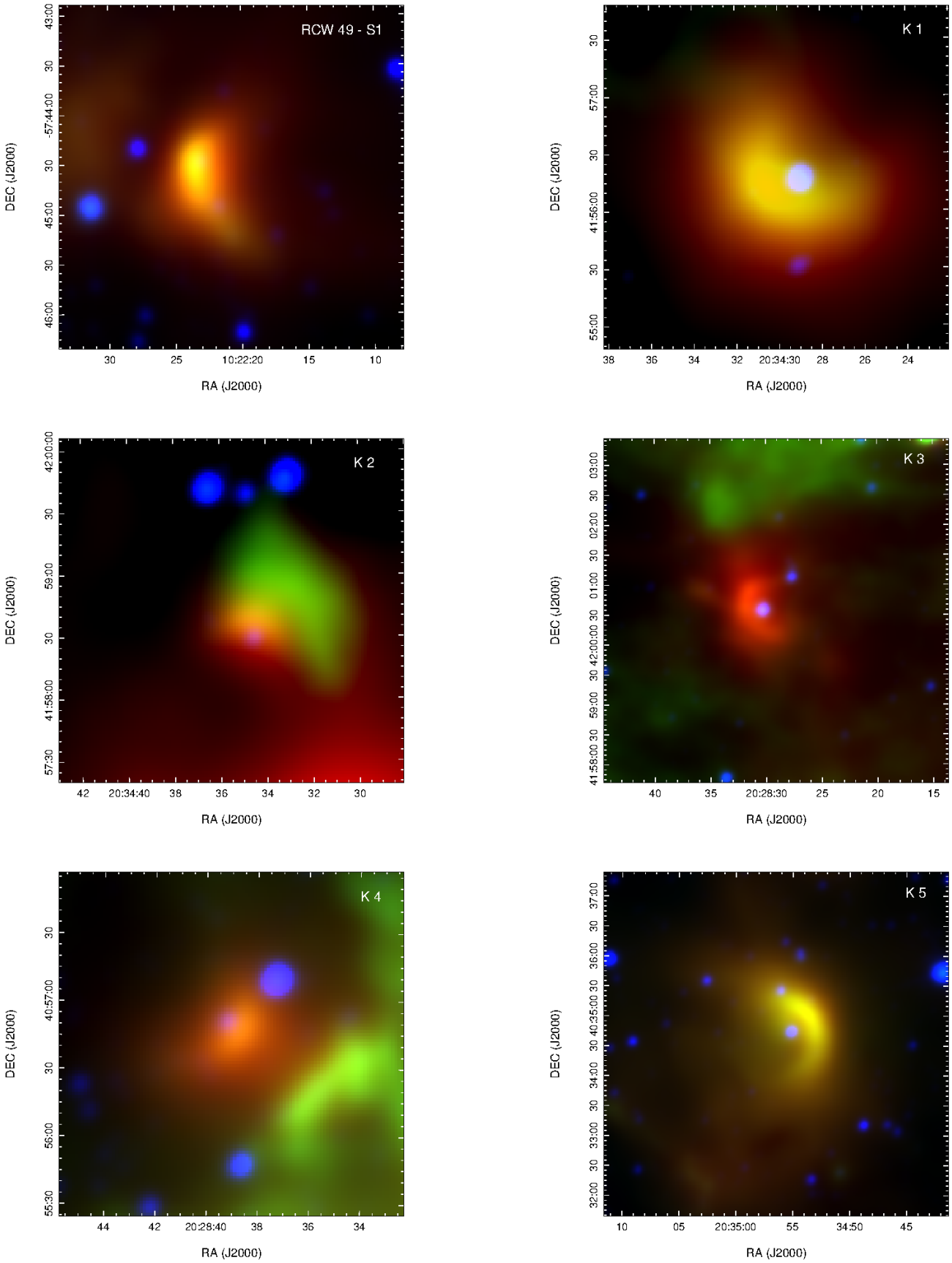

Fig. 7. Group 7 bow-shock candidates WISE images. Red: band 4, 22.2 μm. Green: band 3, 12.1 μm. Blue: band 1, 3.4 μm. The label stands for the name in the final list of E-BOSS r2 BSCs.

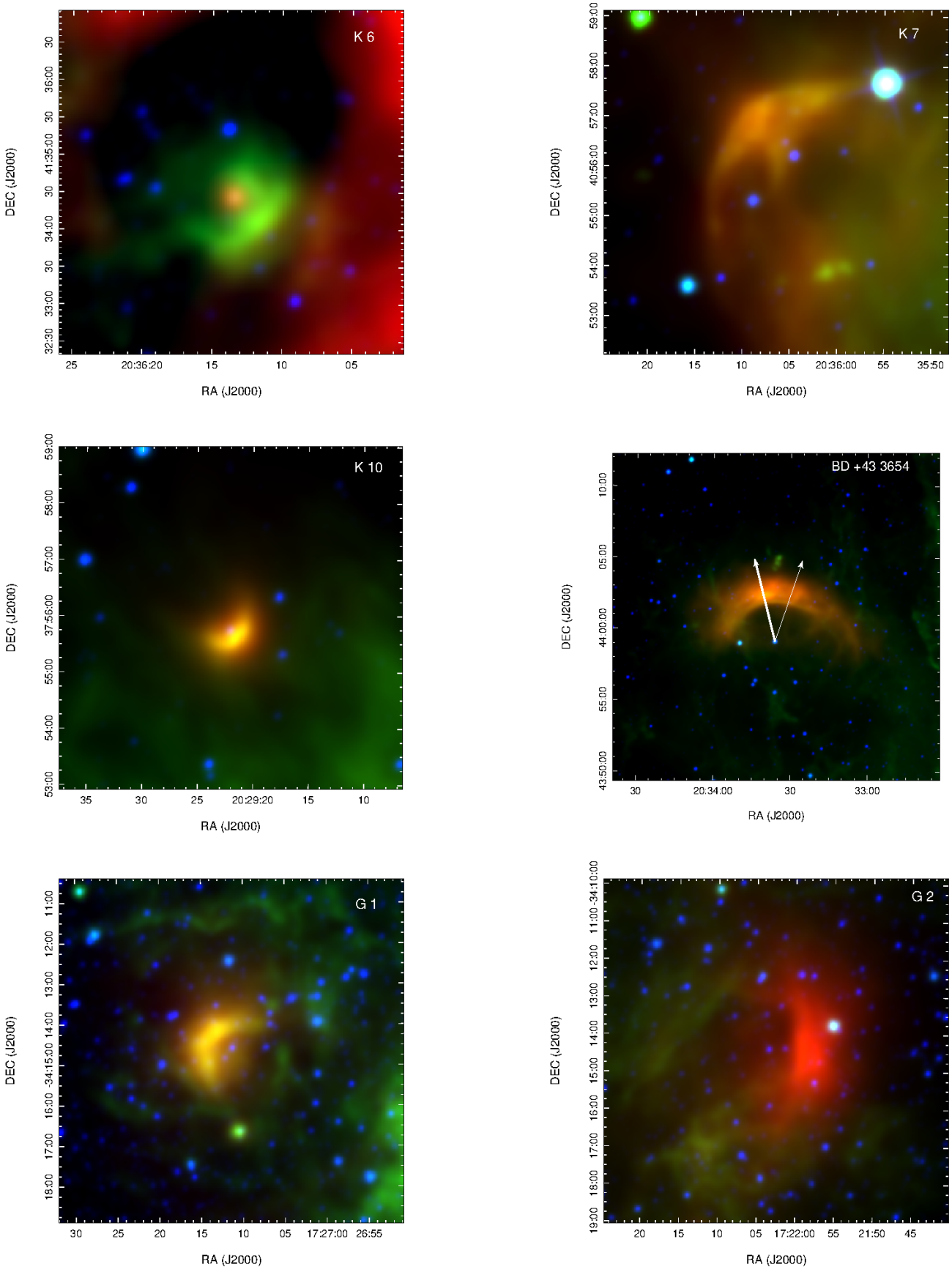

Fig. 8. Group 7 bow-shock candidates WISE images. Red: band 4, 22.2 μm. Green: band 3, 12.1 μm. Blue: band 1, 3.4 μm. The label stands for the name in the final list of E-BOSS r2 BSCs. For BD +43° 3654, we have drawn $\mu_\alpha \cos\delta$ and μ_δ to compose the total μ. The thick vector represent the measured *Hipparcos* proper motions (van Leeuwen 2007), and the thinner vectors stand for the star proper motions but corrected for the ISM motion caused by Galactic rotation. The vector lengths are not scaled with the original values.

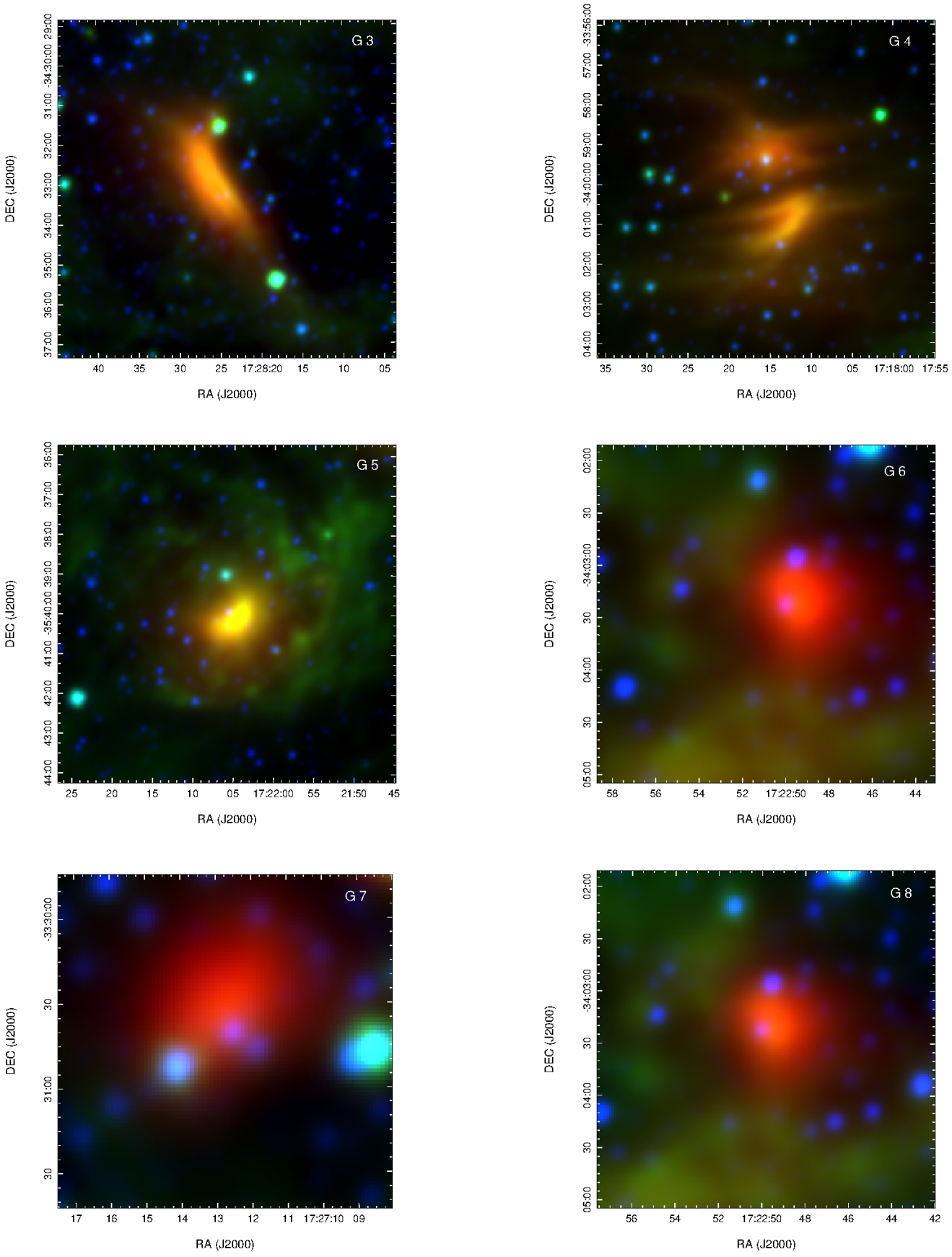

Fig. 9. Group 7 bow-shock candidates WISE images. Red: band 4, 22.2 μm. Green: band 3, 12.1 μm. Blue: band 1, 3.4 μm. The label stands for the name in the final list of E-BOSS r2 BSCs. The BSC labeled G 4 has two structures; we have taken the BSC of the northern one because of the location of the star that might have generated it.

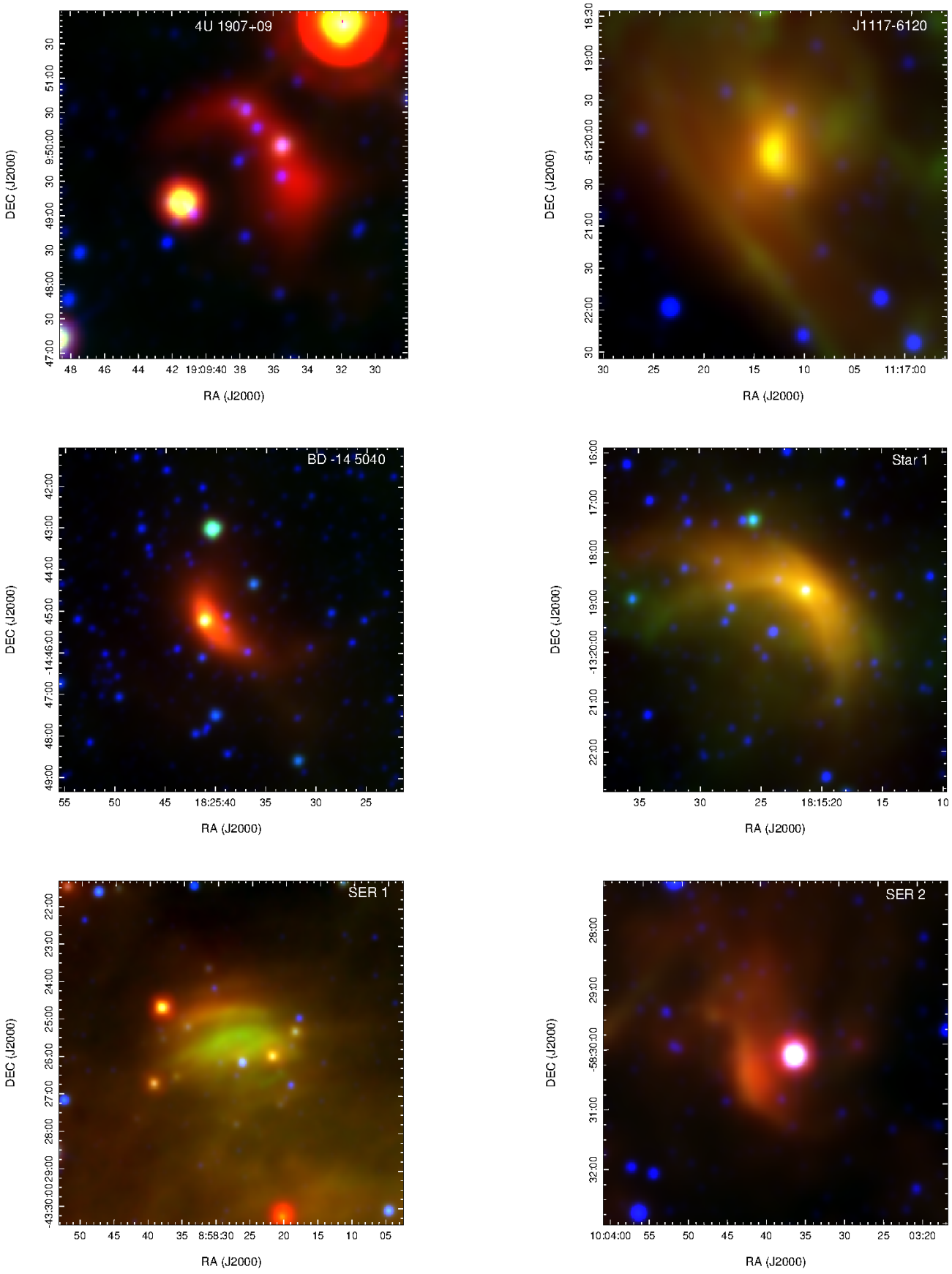

Fig. 10. Group 7 bow-shock candidates WISE images. Red: band 4, 22.2 μm. Green: band 3, 12.1 μm. Blue: band 1, 3.4 μm. The label stands for the name in the final list of E-BOSS r2 BSCs.

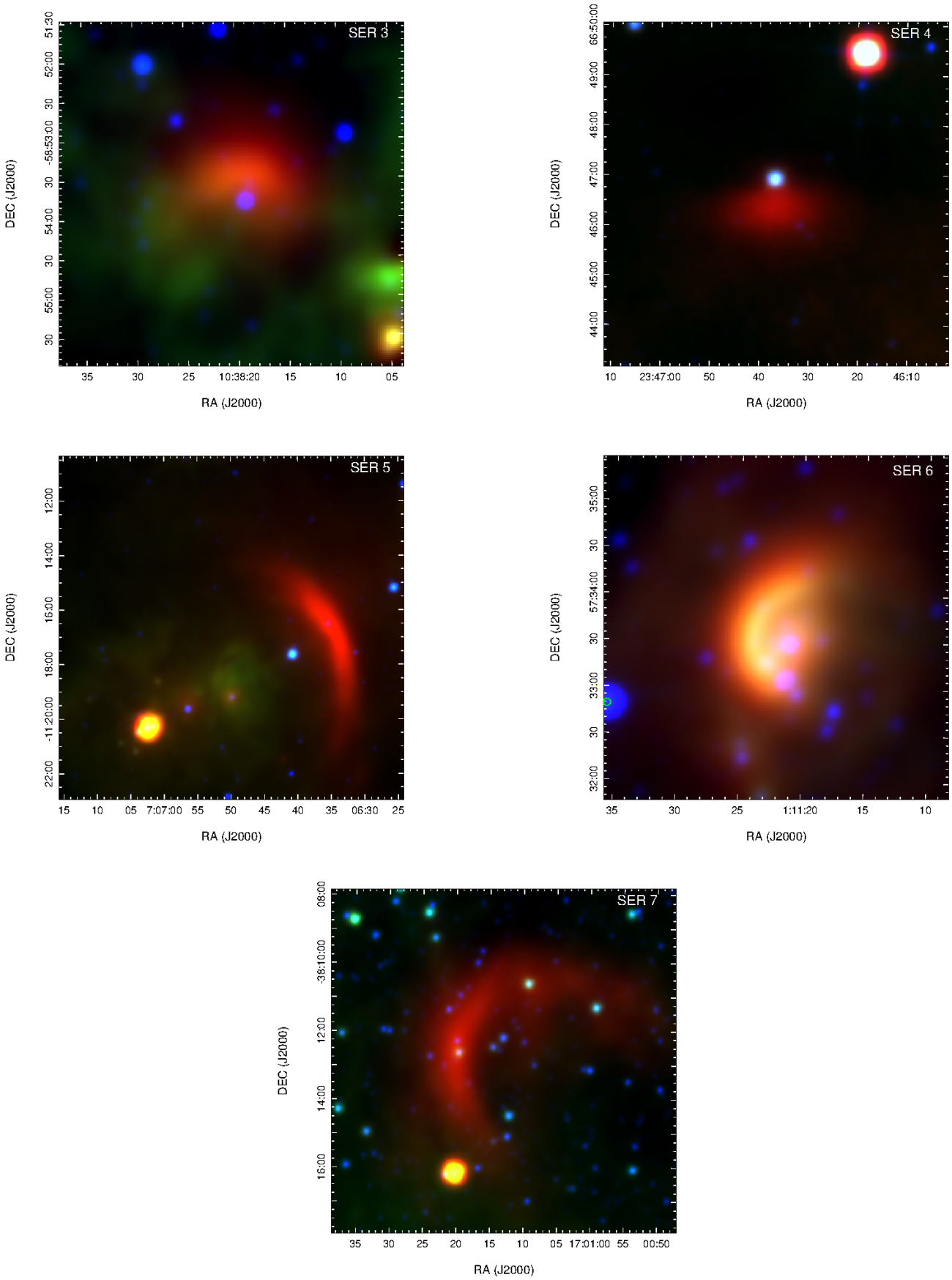

Fig. 11. Group 7 bow-shock candidates WISE images. Red: band 4, 22.2 μm. Green: band 3, 12.1 μm. Blue: band 1, 3.4 μm. The label stands for the name in the final list of E-BOSS r2 BSCs.